Water Resources Research

RESEARCH ARTICLE
10.1029/2024WR039227

Restoring Historic Forest Disturbance Frequency Would Partially Mitigate Droughts in the Central Sierra Nevada Mountains

E. N. Boardman[1], Z. Duan[2], M. S. Wigmosta[2], S. W. Flake[3], M. R. Sloggy[4], J. Tarricone[1,5,6], and A. A. Harpold[1,7]

[1]Graduate Program of Hydrologic Sciences, University of Nevada, Reno, Reno, NV, USA, [2]Pacific Northwest National Laboratory, Richland, WA, USA, [3]Department of Forestry and Environmental Resources, North Carolina State University, Raleigh, NC, USA, [4]Pacific Southwest Research Station, U.S. Forest Service, Riverside, CA, USA, [5]Hydrological Sciences Laboratory, NASA Goddard Spaceflight Center, Greenbelt, MD, USA, [6]NASA Postdoctoral Program, NASA Goddard Space Flight Center, Greenbelt, MD, USA, [7]Department of Natural Resources and Environmental Science, University of Nevada, Reno, Reno, NV, USA

Key Points:

- Restoring historic forest disturbance return intervals can increase water yield by 8%–14% during dry years in the central Sierra Nevada
- Understory largely compensates for reduced overstory transpiration, so 73% of streamflow gains are attributable to reduced interception loss
- Thinner forests can increase headwaters peak flows, but climate uncertainty overwhelms this effect at the reservoir scale

Supporting Information:

Supporting Information may be found in the online version of this article.

Correspondence to:

E. N. Boardman,
eli.boardman@mountainhydrology.com

Citation:

Boardman, E. N., Duan, Z., Wigmosta, M. S., Flake, S. W., Sloggy, M. R., Tarricone, J., & Harpold, A. A. (2025). Restoring historic forest disturbance frequency would partially mitigate droughts in the central Sierra Nevada mountains. *Water Resources Research*, *61*, e2024WR039227. https://doi.org/10.1029/2024WR039227

Received 23 OCT 2024
Accepted 21 MAR 2025

Author Contributions:

Conceptualization: E. N. Boardman, M. S. Wigmosta, M. R. Sloggy, A. A. Harpold
Data curation: E. N. Boardman
Funding acquisition: M. S. Wigmosta, M. R. Sloggy, A. A. Harpold
Methodology: E. N. Boardman, Z. Duan, M. S. Wigmosta, S. W. Flake, M. R. Sloggy, A. A. Harpold
Project administration: M. S. Wigmosta, M. R. Sloggy, A. A. Harpold
Resources: A. A. Harpold

Abstract Forest thinning and prescribed fire are expected to improve the climate resilience and water security of forests in the western U.S., but few studies have directly modeled the hydrological effects of multi-decadal landscape-scale forest disturbance. By updating a distributed process-based hydrological model (DHSVM) with vegetation maps from a distributed forest ecosystem model (LANDIS-II), we simulate the water resource impacts of forest management scenarios targeting partial or full restoration of the pre-colonial disturbance return interval in the central Sierra Nevada mountains. In a fully restored disturbance regime that includes fire, thinning, and insect mortality, reservoir inflow increases by 4%–9% total and 8%–14% in dry years. At sub-watershed scales (10–100 km^2), thinning dense forests can increase streamflow by >20% in dry years. In a thinner forest, increased understory transpiration compensates for decreased overstory transpiration. Consequentially, 73% of streamflow gains are attributable to decreased overstory rain and snow interception loss. Thinner forests can increase headwater peak flows, but reservoir-scale peak flows are almost exclusively influenced by climate. Uncertainty in future precipitation causes high uncertainty in future water yield, but the additional water yield attributable to forest disturbance is about five times less sensitive to annual precipitation uncertainty. This partial decoupling of the streamflow disturbance response from annual precipitation makes disturbance especially valuable for water supply during dry years. Our study can increase confidence in the water resource benefits of restoring historic forest disturbance frequencies in the central Sierra Nevada mountains, and our modeling framework is widely applicable to other forested mountain landscapes.

1. Introduction

Historical fire suppression (Stephens et al., 2016; van Wagtendonk et al., 2018) and anthropogenic climate change (Seidl et al., 2017; Tague & Dugger, 2010) have combined to force North American conifer forests into an unstable ecosystem state (Marlon et al., 2012; Schoennagel et al., 2017). As a result of fire exclusion policies, forests in the Sierra Nevada mountains of California and Nevada (USA) are artificially homogenous and dense (Collins et al., 2011; Dolanc et al., 2014; Taylor et al., 2014), which increases vulnerability to damaging megafires (Goss et al., 2020; Safford et al., 2022; Skinner & Chang, 1996; Steel et al., 2015) and negatively impacts water security (Boisramé et al., 2017b; Stephens, Thompson, et al., 2021). Restoring pre-colonial forest disturbance frequencies and patterns through mechanical thinning and prescribed fire (Kalies & Yocom Kent, 2016; North et al., 2007; Scholl & Taylor, 2010; Stephens, Battaglia, et al., 2021) can increase the resilience of forests (Hessburg et al., 2019; Knapp et al., 2021) and provide societal benefits including reduced catastrophic fire risk (Loudermilk et al., 2016), stabilized carbon storage (Cabiyo et al., 2021; Liang et al., 2018), wood products (Elias et al., 2023; Swezy et al., 2021), increased ecological diversity (Stephens, Thompson, et al., 2021), and increased water yield (Chung et al., 2024; Guo et al., 2023).

Multi-benefit forest management frameworks may help fund disturbance-restoration projects by bundling convergent societal goals and economic incentives to build partnerships (Quesnel Seipp et al., 2023; Stephens, Battaglia, et al., 2021). The Tahoe Central Sierra Initiative (TCSI) is one such partnership, focusing on multi-benefit resilience-based forest management plans for the Truckee, Yuba, Bear, and American River basins

Software: E. N. Boardman, Z. Duan, M. S. Wigmosta, S. W. Flake
Supervision: Z. Duan, M. S. Wigmosta, A. A. Harpold
Validation: E. N. Boardman
Visualization: E. N. Boardman
Writing – original draft: E. N. Boardman, S. W. Flake
Writing – review & editing: E. N. Boardman, M. S. Wigmosta, S. W. Flake, M. R. Sloggy, A. A. Harpold

(Manley et al., 2023). As part of the TCSI, the U.S. Forest Service is assessing the feasibility of environmental markets for ecosystem services such as water supply, carbon storage, and wood products. Several environmental markets could potentially benefit from forest management tactics leading to more frequent tree removals and controlled fire, aligned with partial or full restoration of the pre-colonial disturbance return interval (Maxwell et al., 2022; van Wagtendonk et al., 2018). This target disturbance return interval varies from ∼10 years in lower-elevation and mid-montane areas to ∼30–40 years or longer at high elevations (Maxwell et al., 2022). In this study, we investigate the potential impact of landscape-scale forest disturbance restoration scenarios developed by Maxwell et al. (2022) on water resources in the TCSI region.

The possibility of increased water yield has incentivized forest thinning efforts for decades, but the magnitude and even direction of post-disturbance streamflow changes can vary widely across western North America (Goeking & Tarboton, 2022). Catchment studies have observed that streamflow may increase if forest cover is reduced because of decreased evapotranspiration (ET) (Bosch & Hewlett, 1982; Hibbert, 1967; Troendle & King, 1985). At the landscape scale, however, the hydrological response to vegetation disturbance is more nuanced (Andréassian, 2004), and ET can increase with a thinner canopy (Goeking & Tarboton, 2020) due to a combination of reduced shading (Morecroft et al., 1998), wetter soils (Boisramé et al., 2018), and vegetation regrowth (Perry & Jones, 2016). In their analysis of forest disturbance for 159 watersheds in the western U.S., Goeking and Tarboton (2022) found that energy-limited watersheds (i.e., annual potential ET < precipitation) are more likely to experience increases in streamflow associated with reductions to forest cover compared to more arid watersheds. This mediating effect of aridity on reductions in ET after vegetation disturbance is similarly observed locally in the Sierra Nevada mountains, where more northerly (wetter) watersheds experience larger streamflow gains following disturbance (Saksa et al., 2017). Previous studies in the TCSI region, which is part of the wetter northern Sierra Nevada zone, have predicted substantial increases in streamflow after forest fire or thinning (Guo et al., 2023; Roche et al., 2018, 2020; Saksa et al., 2020). However, prior attempts to quantify landscape-scale streamflow changes usually rely on extrapolation from a few years of pre- and post-disturbance measurements at the plot or small catchment scale (e.g., Roche et al., 2018; Saksa et al., 2020). Landscape-scale forest disturbance is not an instantaneous nor homogenous process, and the hydrological effects of proposed multi-decadal forest treatment plans (Maxwell et al., 2022) are further complicated by the role of climate change in mediating ecohydrology in the coming decades (Tague & Dugger, 2010). In a warmer climate, potential ET may increase, and increasing aridity may reduce streamflow gains (Goeking & Tarboton, 2022).

Seasonal snowmelt controls water resources in much of western North America (Bales et al., 2006), and there have been long-standing efforts to understand how forest management might increase water yield and delay snowmelt runoff (Kattelmann et al., 1983; Troendle, 1983). A majority of studies analyzed by Varhola et al. (2010) and Goeking and Tarboton (2020) associate thinner forests with increased snow accumulation and faster ablation rates. However, forest-snowpack relationships exhibit considerable variability due to complex mass and energy interactions that are mediated by climate and topographic controls. Reduced canopy interception tends to increase accumulation, particularly in areas with snowfall events near or below the canopy storage capacity (Boon, 2012; Storck et al., 2002; Winkler et al., 2012). However, increased shortwave radiation reaching the snowpack in thinner forests can accelerate ablation, particularly on southern aspects (Ellis et al., 2011; Harpold et al., 2014; Tennant et al., 2017). Conversely, in relatively warm climates, decreased longwave radiation from canopy removal can enhance snow retention in newly created open areas (Safa et al., 2021). Darker snow albedo in post-fire forests can compound the effect of reduced shading, further accelerating snow ablation (Gleason et al., 2013, 2019). Due to the competing interaction of interception and shading effects, as well as additional factors including wind and thermal radiation from trees, many studies conclude that the snowpack response to disturbance is a complex function of the local conditions and fine-scale forest structure (e.g., Harpold et al., 2020; Stevens, 2017; Sun et al., 2018; Troendle, 1983). In the TCSI region considered in this study, high resolution lidar and modeling studies indicate that snow accumulation and meltwater inputs increase or decrease in different areas depending on the interaction of canopy structure with solar radiation and wind (Lewis et al., 2023), and opening gaps in dense canopies will promote snow accumulation and reduce ablation (Piske et al., 2024).

The effect of forest disturbance on net ET, and hence water yield, depends on a cascade of complex factors (Adams et al., 2012; Moore & Heilman, 2011). The different vapor loss components of ET (i.e., transpiration and

evaporation or sublimation from interception storage) can be categorized depending on whether they are expected to increase or decrease in a thinner forest (see Figure 1 of Goeking and Tarboton (2020)). Declines in transpiration have been observed following tree mortality (Bales et al., 2018), which can reduce the soil moisture deficit and thus support additional streamflow generation from future precipitation (Boisramé et al., 2018; He et al., 2013; Troendle, 1979). However, increased soil water availability sometimes supports higher transpiration rates from the remaining trees that would otherwise be water-limited, thereby capping streamflow gains during dry periods (Boisramé et al., 2019). Moreover, aerodynamic effects and reduced shading can create a more arid microclimate and contribute to increases in ET from remaining vegetation (Ma et al., 2010; Meili et al., 2024; Morecroft et al., 1998; Rambo & North, 2009), further limiting the streamflow response to disturbance (Biederman et al., 2014; Meili et al., 2024). As a result, watershed-scale vapor loss can increase, decrease, or remain relatively unchanged following severe forest disturbance (Goeking & Tarboton, 2020). Predicting the landscape-scale response to proposed management plans requires modeling the interaction of topography, soils, snow, and vegetation over decades of planned forest treatments under a changing climate.

As climate change increases the flood risk in Sierra Nevada watersheds (Huang & Swain, 2022), the potential for forest disturbance to exacerbate peak flow magnitude requires consideration. Forest disturbance generally increases peak streamflow (Goeking & Tarboton, 2020), but this response is dependent on the interaction of many processes. At small watershed scales, peak flows tend to increase after disturbance due to interactions between elevated antecedent water tables, reduced interception, increased snow accumulation, and faster snowmelt (Lewis et al., 2001; Moore & Wondzell, 2005; Pomeroy et al., 2012). Additionally, natural or prescribed fires may contribute to peak flows through increased surface runoff from hydrophobic soils (Certini, 2005). The ancillary effects of mechanical thinning such as soil compaction (Startsev & McNabb, 2000) or the cutting of new forest roads can similarly alter flow paths and increase peak flows (Bowling & Lettenmaier, 2002; King & Tennyson, 1984). Peak flow increases on the order of 50% or more have been observed after forest disturbance in catchments up to a few square kilometers in area (Moore & Wondzell, 2005), but peak flow impacts in larger-scale basins remain uncertain. Jones and Grant (1996) use the variable timing of forest harvest to propose a statistical argument that forest disturbance may contribute to substantially higher peak flows in watersheds as large as 600 km^2 in the Oregon Cascade Range, though this finding is contradicted by reanalysis of the same data by Thomas and Megahan (1998). Quantifying the potential risks of more frequent forest disturbance in the Sierra Nevada requires modeling short-term hydrological responses (e.g., one-day peak flow) over multi-decadal time horizons.

In this study, we address two of the unsolved problems in hydrology, namely the impact of land cover change on water fluxes and the spatial variability in hydrologic extremes in response to this change (Blöschl et al., 2019) by incorporating the outputs of a forest ecosystem model into a distributed hydrological model to simulate the spatially explicit hydrological effects of landscape-scale forest management scenarios. Forest management scenarios considered here are based on input from the broader TCSI partnership (Maxwell et al., 2022), so our hydrological investigation is uniquely grounded in detailed and plausible management alternatives in a landscape-scale forest planning exercise. Using a novel combination of two state-of-the-art models and a new Bayesian calibration method, we seek to answer the following questions: (a) How much additional water yield would result from partial or full restoration of the historic forest disturbance return interval in the central Sierra Nevada, and which factors control variability in the sub-watershed response? (b) Could more frequent forest disturbance increase peak flows in ways that might accentuate flood risks to small- or large-scale infrastructure? (c) How do the sources of uncertainty inherent in multi-decadal simulations (climate, model uncertainty, and other unknowns) affect water resource planning?

2. Methods

First, we set up and calibrate a hydrological model using historical streamflow, water yield, and snow data. Second, we set up and calibrate a forest ecosystem model to simulate vegetation responses to different forest management scenarios. Third, we run the hydrological model to the end of the century using climate projections and vegetation states from the forest ecosystem model. Figure 1 outlines the interaction between these three main components of our study. The following sections address each of the components in detail.

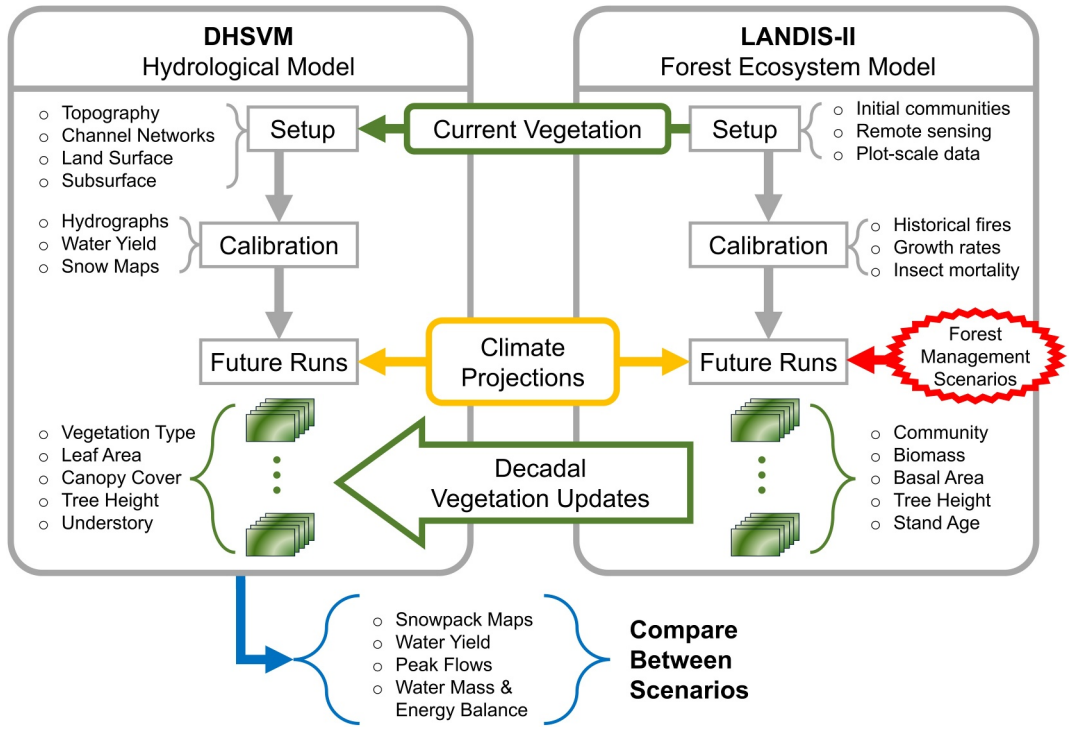

Figure 1. Methodological flowchart for simulation procedures used in this study. Vegetation states simulated by the forest ecosystem model are used to update the hydrological model under different forest management scenarios.

2.1. Hydrological Modeling

A physics-based, distributed-parameter approach to hydrological modeling enables us to quantify the interacting effects of forest disturbance on hydrological processes and evaluate spatial heterogeneity in the watershed response to forest management scenarios. The Distributed Hydrology Soil Vegetation Model (DHSVM) was developed by Wigmosta et al. (1994, 2002) to simulate mountain watersheds with a particularly robust treatment of forest ecohydrological processes, such as overstory and understory interception and transpiration. DHSVM solves a water mass and energy balance on a two-dimensional grid, typically at high spatial resolution (90 m in this study) on a sub-daily timestep (3 hr in this study). A two-layer one-dimensional mass/energy balance snowpack model simulates accumulation, ablation, and snowmelt/rain percolation based on the vegetation and weather microclimate of each grid cell. The model represents vegetation with a two-layer "big leaf" approach that enables the separate calculation of overstory and/or understory interception of rain and snow, evaporation or sublimation from interception storage, and transpiration from three root zone soil layers in each grid cell. Streamflow in DHSVM is primarily generated from saturated subsurface flow where the water table intersects a spatially explicit channel network, though overland flow can also occur. Soil moisture and groundwater are recharged by surface infiltration, and water in the saturated zone moves laterally through a shallow aquifer based on two-dimensional hydraulic gradients, approximated in this study from the local surface topography and spatially variable soil hydraulic properties. Compared to other landscape-scale process-based ecohydrology models, DHSVM is notable for the high grid-scale resolution of its water mass and energy balance and the high fidelity of its ecohydrological processes, which makes it particularly suitable for simulating the hydrological effects of heterogeneous forest disturbances (Beckers et al., 2009; Sun et al., 2023).

2.1.1. Hydrological Model Setup

We combine literature review and a variety of spatial data sets to set up DHSVM for the study region in the central Sierra Nevada mountains. The TCSI area includes four adjoining watersheds, as shown in Figure 2: the Truckee River (2,273 km^2, mean elevation 2,100 m), the Yuba River (3,435 km^2, mean elevation 1,305 m), the Bear River (585 km^2, mean elevation 821 m), and the American River (4,812 km^2, mean elevation 1,350 m). Topography is represented using elevations from the Shuttle Radar Topography Mission (SRTM; Farr et al., 2007). Stream

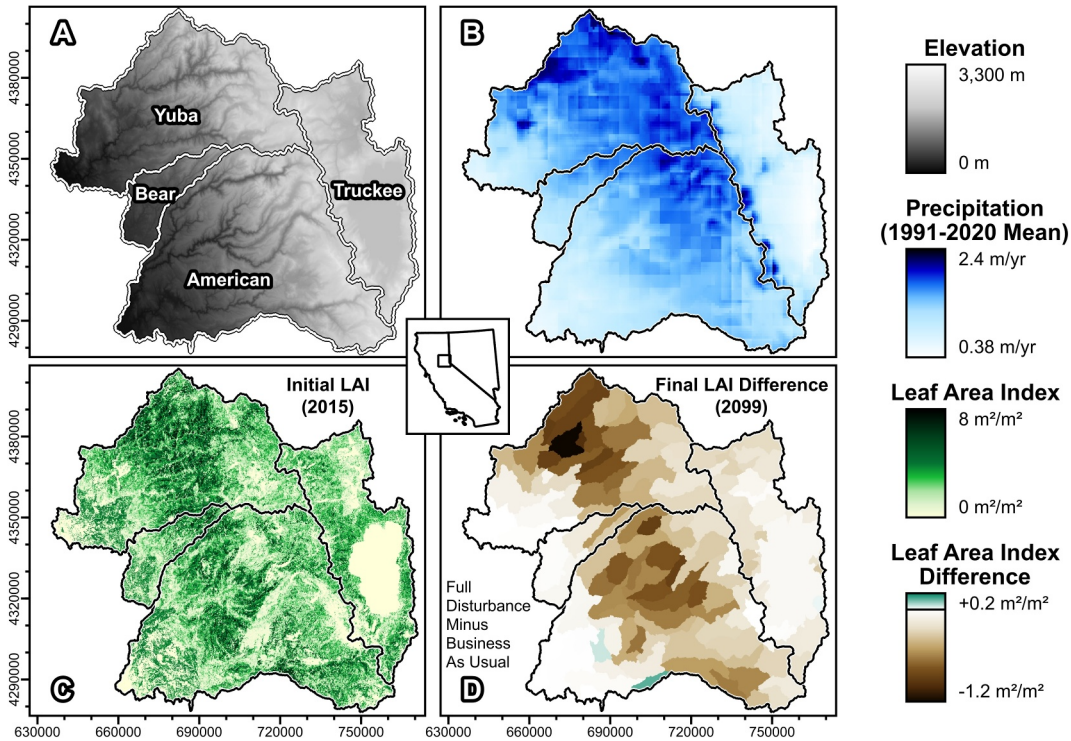

Figure 2. Maps of the Tahoe-Central Sierra project area: (a) digital elevation model; (b) mean yearly precipitation; (c) pre-treatment (historical) leaf area index (LAI); (d) final LAI difference between the full disturbance (S6) and business-as-usual (S2) management scenarios aggregated by sub-watershed. Inset map shows the study area location in the U.S. states of California and Nevada. All map coordinates are in UTM zone 10N, and tick marks indicate 10 km.

networks are initiated with a minimum catchment area of 0.1 km^2, which is consistent with imagery and the National Hydrography Database (NHD) channel network (U.S. Geological Survey, 2019). Textural soil data required for DHSVM are derived from POLARIS (Chaney et al., 2019), a high-resolution probabilistic remapping of the Soil Survey Geographic (SSURGO) Database (Soil Survey Staff, 2022). The multi-layer POLARIS data are vertically aggregated to three root-zone depth layers up to 1.2 m depth (Jackson et al., 1996), plus a deep layer. The Supporting Information S1 includes an exhaustive description of inputs to DHSVM and their estimation for this study, and relevant code is available online (see Availability Statement).

The parameterization of vegetation in DHSVM requires particular attention to robustly estimate the effects of forest disturbance. Spatially explicit maps of vegetation type, canopy fractional cover, overstory monthly leaf area index (LAI), tree height, and dense understory presence are derived from outputs of the forest ecosystem model (Section 2.2). Where dense understory is not indicated, we assume a light understory presence beneath the forest canopy based on anecdotal field experience from 18+ sites distributed throughout the study region, which indicates a typical lack of bare soil. Understory is parameterized with a constant LAI of 3 m^2/m^2 for dense understory or 1 m^2/m^2 for light understory based on field estimates of LAI for shrub ecosystems common to the study area (Hughes et al., 1987; McMichael et al., 2004). Through manual sensitivity tests, we find that most vegetation parameters are insensitive to minor perturbations in the study region, so these parameters are maintained at baseline values used elsewhere in the DHSVM literature. One particularly sensitive parameter is the minimum stomatal resistance, which controls overstory transpiration for each vegetation type. We conduct a review of 18 species-level stomatal conductance field studies to estimate minimum resistance values and uncertainties for 15 distinct DHSVM vegetation types with at least two literature estimates per type (see Supporting Information S1). Canopy interception parameters are estimated from numerous field studies using the literature review summaries compiled by Link et al. (2004) for rain and Martin et al. (2013) for snow. Finally, abiotic land surfaces including water, urban, and rock types are mapped using the National Land Cover Database (NLCD; Dewitz and U.S. Geological Survey, 2019) and represented in DHSVM with impermeable areas and detention storage (Cuo et al., 2008).

Meteorological forcing data for DHSVM are generated using a variety of spatiotemporal disaggregation techniques. Historic meteorological data are obtained from gridMET (Abatzoglou, 2013), and future climate projections are obtained from the analogous Multivariate Adaptive Constructed Analogs (MACA) downscaled global circulation model (GCM) data set (Abatzoglou & Brown, 2012). Both climate data sets provide daily precipitation, minimum/maximum temperature, and wind speed at 4 km resolution. The model requires inputs of precipitation, air temperature, relative humidity, wind speed, incoming shortwave radiation, and incoming longwave radiation. We temporally disaggregate the daily data to the 3-hr DHSVM timestep and simulate the additional required variables using MetSim (Bennett et al., 2020), which is based on the MTCLIM model (Hungerford et al., 1989). Precipitation is assumed constant within each day, which is a reasonable assumption for the multi-day cold-season storms typical of the central Sierra Nevada (e.g., Huning & Margulis, 2017), but we acknowledge that this assumption could affect assessments of rain-driven peak flow events. We spatially disaggregate 4 km gridMET precipitation data using monthly redistribution maps calculated from 800 m PRISM normals (PRISM Climate Group, 2022) to exactly preserve the spatial mass balance of the 4 km data while redistributing precipitation approximately proportional to the monthly PRISM normals within each 4 km cell (Figure 2b). Preserving the exact gridMET precipitation mass balance is a priority in this study for the sake of consistency with the gridMET forcing data used for LANDIS-II, so we eschew common downscaling techniques that are not mass-preserving, such as bilinear interpolation. Temperature data are spatially disaggregated to the 90 m DHSVM grid scale using spatially variable monthly lapse rates calculated by linear regression of elevation versus PRISM monthly temperature normals for the 25,800 m cells within each 4 km gridMET cell. In the study region, there are 193 gridMET cells covering the Truckee watershed, 295 covering the Yuba watershed, 65 covering the Bear watershed, and 385 covering the American watershed. Baseline DHSVM parameters controlling snowpack accumulation and ablation are set based on the results of Sun et al. (2019) for the Sierra Nevada region.

2.1.2. Hydrological Model Calibration

We refine our baseline setup of DHSVM with calibration of key parameters. Manual sensitivity tests reveal seven parameters that are sensitive to perturbation within the a priori uncertainty range of available data: mean soil depth [m], hydraulic conductivity [m/s], the exponential decrease in hydraulic conductivity with depth [−], porosity [%], minimum stomatal resistance [s/m], the maximum air temperature for snowfall [°C], and the melt-season albedo decay rate [−]. Soil depth is calibrated using an offset applied to a baseline pattern based on topographic curvature (Patton et al., 2018) to generate a mean soil depth between 1.3 and 4 m based on the minimum required to satisfy the rooting depth and upper-bound sensitivity tests. Hydraulic conductivity and porosity are calibrated between the 5th, 50th, and 95th percentile values for each grid cell and soil layer provided by the POLARIS data (Chaney et al., 2019). Single-valued parameters are calibrated over a prior range determined from variability observed in the literature or manual sensitivity tests, as outlined in the Supporting Information S1. All parameters and maps are maintained within plausible physical ranges, and all four major TCSI basins are calibrated together to improve generality.

To quantify uncertainty in key hydrological processes, we evaluate six objective functions targeting different hydrological signatures. The selected objective functions are daily streamflow Nash-Sutcliffe Efficiency (NSE), log-scale NSE for two sets of sub-watersheds exhibiting comparatively high or low baseflows, root mean squared error (RMSE) for yearly water yield at large scales, RMSE for 95th-percentile high flows at large scales, and pixel-wise RMSE for yearly peak SWE. The calibration period is defined as water years 2012–2017 for streamflow data (not counting one year of model spin-up) in order to capture a range of variability, including a multi-year drought (2013–2015) and one of the wettest years in recent decades (2017). Unimpaired or reconstructed daily streamflow timeseries are obtained for 10 stream gauges in the Truckee and Yuba watersheds (U.S. Geological Survey, 2022; refer to calibration figures in Supporting Information S1 for gauge numbers). Large-scale flows are constrained with reconstructions of natural streamflow at the YRS flow point (California Department of Water Resources, 2022). Yearly pixel-wise peak SWE maps are calculated for the Yuba and Truckee watersheds from the Margulis et al. (2016) snow reanalysis for water years 2011–2016.

We apply multi-objective Bayesian optimization to the sensitive parameters identified previously in order to minimize errors in each objective function and quantify residual hydrological uncertainty. In Bayesian optimization, objective functions are modeled using stochastic processes as surrogates for the underlying model (DHSVM in our case), which boosts calibration efficiency (Jones et al., 1998). Starting with an initial minimax

Latin hypercube sample of the seven-dimensional parameter space (Morris & Mitchell, 1995, implemented by Dupuy et al., 2015), we use Gaussian Process regression (Rasmussen & Williams, 2008, implemented by Roustant et al., 2012) to build surrogate models of each objective, and optimize the expected hypervolume improvement of subsequent parameter sets (Emmerich et al., 2011, implemented by Binois & Picheny, 2019) with parallel particle swarm optimization (Kennedy & Eberhart, 1995, implemented by Zambrano-Bigiarini et al., 2013). After testing a total of 300 unique parameter sets during 6 rounds of optimization, we identify Pareto-efficient designs, which constitute the set of models where improving one objective requires worsening another. From this Pareto set of calibrated models, we select three high-performing models that are representative of the tradeoffs between objective functions and the residual uncertainty in calibration parameters (Figures S1–S3 in Supporting Information S1). We validate the selected models over water years 2006–2011. During validation, we expand our objective functions to include two additional stream gages and reconstructed natural flows in the American River watershed at the AMF/NAT flow point below Folsom Lake (California Department of Water Resources, 2022).

2.1.3. Hydrological Model Future Runs

We simulate the long-term hydrological effects of forest disturbance by running DHSVM subject to future climate projections and updating vegetation maps to reflect spatiotemporal heterogeneity associated with forest disturbances, management, and regrowth. We select the CNRM-CM5 (Voldoire et al., 2013) and MIROC5 (Watanabe et al., 2010) climate projections since these models represent endmembers for fire weather in the central Sierra Nevada study region (Maxwell et al., 2022), with CNRM-CM5 representing a relatively wet scenario, and MIROC5 representing a relatively dry scenario. We select the RCP-8.5 pathway for both GCMs since this higher-emissions scenario fits likely behaviors in the near to mid-future (Schwalm et al., 2020). On average within the project area, the CNRM-CM5 climate projection has a temperature trend (Sen, 1968) of 0.062°C/yr, amounting to a 5.3°C increase over the 85-year simulation period, with mean precipitation of 597 mm/yr. The MIROC5 climate has a temperature trend of 0.045°C/yr, amounting to a 3.9°C increase over 85 years, with 456 mm/yr mean precipitation (24% less than CNRM-CM5). GCM projections are further disaggregated and downscaled from the Abatzoglou and Brown (2012) MACA data set using the same methodology outlined above for consistency with the forcing data on the historic calibration and validation periods.

The effect of ongoing forest disturbance is represented in DHSVM with updated maps of vegetation type, canopy fractional cover, overstory LAI, tree height, and dense understory presence every 10 years. Updated vegetation maps are ingested into DHSVM on October 1st 5 years prior to the date that they represent. Offsetting the dates with this approach enables DHSVM to simulate hydrological conditions for each set of vegetation maps over a 10-year period centered on the year corresponding to the updated vegetation maps. More frequent (e.g., yearly) updates of the DHSVM vegetation maps could better resolve rapid changes near the beginning of the treatment period, but we find that decadal updates can satisfactorily resolve relatively slow trends in the forest landscape after the first decade of treatment.

2.2. Forest Ecosystem Modeling

To model change in vegetation over time and in response to climate and management, we used the LANDIS-II forest landscape model (Scheller et al., 2007) with parameterization following Maxwell et al. (2022). LANDIS-II is a flexible modeling framework that allows for varying extensions to model vegetation dynamics and disturbance in a spatially explicit gridded format allowing communication among cells (e.g., by seed dispersal or fire spread). In this study, we also use the Net Ecosystem Carbon and Nitrogen (NECN v6.9) succession extension (Scheller et al., 2011). NECN is a mechanistic succession model which tracks cohorts of trees (each with associated age, species, and biomass) as they grow, reproduce, recruit, and senesce. Cohort growth and establishment depend on site conditions (e.g., climate, soils) and competition with other cohorts for water, growing space, and soil nitrogen. NECN tracks carbon and nitrogen through multiple biomass and soil compartments. In NECN, climate has emergent effects on ecosystem processes through its impact on vegetation growth, respiration, and soil carbon dynamics. All model parameters and installers needed to reproduce our TCSI forest ecosystem model are available online (see Data Availability Statement section).

2.2.1. Forest Ecosystem Model Setup and Calibration

The initial (year 0) landscape of the LANDIS-II model is derived from multiple data sources. Initial vegetation conditions are generated from Forest Inventory and Analysis (FIA) plots (Burrill et al., 2021) imputed from Landsat remote sensing products with soil data from SSURGO. We model several key disturbance processes, including fire (natural ignition and prescribed), insect pests, and harvest (through implementation of the management scenarios).

To model wildfire and prescribed fire, we use the Social-Climate-Related Pyrogenic Processes and their Landscape Effects (SCRPPLE v3.2.3) extension (Scheller et al., 2019), a data-driven empirical model of fire spread, fire intensity, and tree mortality. SCRPPLE simulates fire spread, intensity, and mortality depending on fuels, weather, and topography. The fire parameters are calibrated to ignitions data (Short, 2021), daily fire perimeters from the National Interagency Fire Center (NIFC, 2019) and fire severity maps from Monitoring Trends in Burn Severity (Eidenshink et al., 2007). Tree mortality is parameterized using the Fire and Tree Mortality Database (Cansler et al., 2020). For details, refer to the appendix of Maxwell et al. (2022).

Insect pests are simulated using the Biomass Biological Disturbance Agents (Biomass-BDA) extension, modified from BDA v2.1 (Sturtevant et al., 2004), which simulates outbreaks of pests and pathogens as a spatially contagious process dependent upon climate and host availability. We simulate fir engraver (Scolytus ventralis), Jeffrey pine beetle (Dendroctonus jeffreyi), mountain pine beetle (D. ponderosae), and western pine beetle (D. brevicomis), as well as white pine blister rust (Cronartium ribicola). We calibrate outbreak patterns using USFS Aerial Detection Survey and Ecosystem Disturbance and Recovery Tracker data (Koltunov et al., 2020). The extent and severity of outbreaks is an outcome of climate, host tree density, and spatial patterning, allowing for complex interactions among climate, vegetation, management, and hydrology (Scheller et al., 2018).

2.2.2. Forest Management Scenarios

We utilize several previously developed scenarios (Maxwell et al., 2022) to represent a range of management activities ranging from very little management to approximately full restoration of a natural disturbance return interval. The spatially variable target return interval is most frequent on mid-elevation western slopes, with a recurrence rate of ∼10 years. The scenarios' overall objectives are to restore forest ecosystems to a state that is more similar to their character prior to fire exclusion. The scenarios attempt to restore a low- or mixed-severity fire regime by reintroducing disturbances in the form of prescribed fire or thinning from below. The proportion of the landscape treated per year depends upon the historical fire-return interval of the management zone (see Maxwell et al., 2022; Figure 2), but ranges from ∼1% to ∼6% per year across the whole landscape. We implement harvests using the Biomass-Rank Biomass Harvest extension, a modification of Biomass Harvest that allows greater flexibility in selecting locations to harvest based on their biomass. Management zones are developed using land ownership and land use, slope steepness, and historical fire return interval data from LANDFIRE (U.S. Department of the Interior, 2016). Within all scenarios, private lands are managed as business-as-usual, with pre-commercial thinning and clearcuts on private timberlands. The wildland-urban interface (WUI) Defense zone (within 400 m of settlements) is also treated for fuel reduction in all scenarios. The scenarios are described in detail by Maxwell et al. (2022) and summarized here. Note that the scenario names given here are selected for interpretability with reference to our hydrological results, and the concept of "business-as-usual" is not prescriptive but rather reflects a baseline level of management in the simulations.

1. *Reduced treatment*. Management is restricted to fuel treatments within the WUI Defense zone (within 400 m of settlements) and private lands. This scenario represents a substantial reduction in general forest treatment compared to present-day management.
2. *Business-as-usual (BAU)*. This scenario is designed to closely match management practices in the present and recent past, including private land management and management of general forests as recorded in USFS and CalFire databases.
3. *Partial disturbance with less fire*. In this scenario, treatments are extended to general forest and roadless areas. Almost all treatments are either mechanical thinning or hand thinning, depending upon the slope steepness and land use category. Prescribed fire is used for 5% of treatments on general forest land and 20% of treatments in roadless areas.
4. *Partial disturbance*. This scenario is similar to Scenario 3, but it replaces 20% of the thinning treatments in the WUI Threat zone with prescribed fire.

5. *Full disturbance with less fire*. This scenario and Scenario 6 attempt to replicate the historical disturbance return interval (~6% of the landscape treated per year). The types of treatment and kinds of stands treated are identical to Scenario 4, but the area treated per year is greater.
6. *Full disturbance*. Compared to Scenario 5, this scenario increases the amount of prescribed fire: 30% of treatments in general forest and roadless areas use fire rather than mechanical thinning treatments.

2.2.3. Forest Ecosystem and Hydrological Model Linkage

In order to assess the emergent effects of forest management and disturbance on water resources, we translate outputs from LANDIS-II into suitable inputs for DHSVM. LANDIS-II generates several outputs natively which can be directly used in DHSVM, including LAI (Figure 2c) and species composition (Figure S14 in Supporting Information S1), but other outputs require further processing. To create inputs for fractional canopy cover, we use regression models from FIA data. For details, refer to the appendix of Zeller et al. (2023). Because the LANDIS-II model is parameterized from forest inventory data, understory vegetation is underrepresented in the vegetation layers, which could bias the hydrological model. To impute understory vegetation cover, we use FIA data to create beta regression models predicting understory shrub cover as a function of tree biomass, tree age, canopy cover, and forest type. The beta regression model achieves a fair model fit (pseudo-$R^2 = 0.20$, RMSE = 0.22). We classify sites as having dense understory if the regression model predicts understory shrub cover exceeding 20%. This binary classification has a Cohen's kappa of 0.24, suggesting fair agreement. Sites without a shrub understory have an assumed light understory cover in DHSVHM, typical of grasses and forbs in the study area, as discussed in the hydrological modeling section. Although the empirical model used to distinguish light/dense understory only achieves fair skill, we expect that classification model errors have a limited effect on our DHSVM results since all forested areas are assumed to have at least some understory.

2.3. Output Processing and Scenario Comparisons

Comparing simulated watershed behaviors between different management scenarios enables us to attribute variable hydrological dynamics to forest management actions. Differences in modeled maps of yearly pixel-wise peak SWE and snowmelt timeseries can quantify forest disturbance impacts on the snowpack. We use simulated streamflow timeseries to estimate additional reservoir inflow volumes attributable to forest disturbance, and we construct flow duration curves (Vogel & Fennessey, 1995) to assess impacts on the high flow regime. Finally, aggregated timeseries of water mass balance fluxes enable us to calculate differences in the partitioning of landscape-average yearly overstory and understory transpiration, overstory and understory interception loss, and streamflow generation.

We analyze the effects of forest disturbance on local streamflow generation and peak flows using sub-watershed daily streamflow timeseries. During each DHSVM run, we save streamflow records at 139 selected pour points approximately corresponding to the HUC-12 watersheds represented in the NHD watershed boundary data set (U. S. Geological Survey, 2019). We calculate yearly local streamflow generation for each sub-watershed by subtracting streamflow contributions from any upstream tributaries. Comparing streamflow generation in different management scenarios isolates the effect of forest disturbance. To analyze peak flow effects, we compute the Sen's slope (Sen, 1968) for one-day yearly peak flows in each sub-watershed across the full 85-year period. By differencing the peak flow trends for each sub-watershed under different management scenarios, we ascertain the effect of forest disturbance on one-day yearly peak flows. This approach isolates the effects of each management scenario by removing climate-induced peak flow trends from the business-as-usual scenario.

To investigate peak flow connections to forest disturbance, we isolate major storm runoff events and compare contemporaneous water balance fluxes between different management scenarios. Since we model the study region with four separate watershed domains, three DHSVM models, and two GCMs, we obtain a total of 24 watershed-aggregated timeseries. In each timeseries, we identify yearly peak flow dates across the 85-year simulation period. For peak flow events preceded by multiple days of continuous precipitation, we define a storm period extending from the first day with non-negligible precipitation through the day of the yearly peak flow. For each such event, we calculate precipitation intensity as the mean daily precipitation rate during the storm period. For the 10 highest-intensity precipitation events prior to yearly peak flows in each combination of watershed, DHSVM model, and GCM, we calculate storm-total interception by subtracting the total overstory and understory interception storage (rain plus snow) on the first day of the continuous storm period from the total

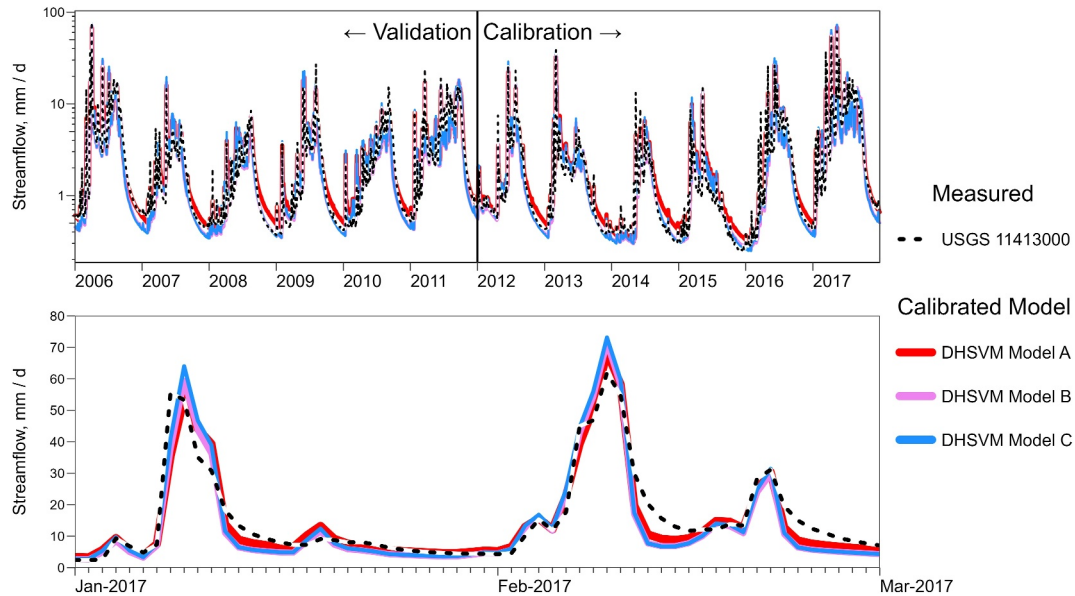

Figure 3. Example calibration and validation hydrographs for Distributed Hydrology Soil Vegetation Model. The North Yuba (USGS station 11413000) is the largest gauged watershed in the study area that has negligible upstream diversion or flow regulation. The model is calibrated on a total of 10 watersheds and validated on a total of 12 watersheds (refer to Supporting Information S1 for additional calibration and validation hydrographs).

interception storage on the peak flow date. We similarly calculate cumulative interception vapor loss, snowpack outflow, and snow energy balance fluxes over the same storm periods. The selected "storm" periods have storm-total mean precipitation of 404 mm at an average rate of 66 mm/d.

3. Results

3.1. Hydrological Model Calibration and Validation

We select three Pareto-efficient DHSVM parameter sets from our multi-objective Bayesian calibration based on tradeoffs between simulation accuracy for the snowpack, baseflows, yearly water yield, and high flows. Model A achieves the highest area-weighted daily NSE across all calibration watersheds, Model B has the lowest RMSE for large-scale high flows, and Model C has the lowest yearly water yield RMSE subject to the requirements of daily NSE >0.8 and high-flow daily RMSE <80 m^3/s. The three selected models are Pareto-efficient for all six calibration objective functions and representative of the residual uncertainty in the calibration parameter space. Model A is notable for having relatively low porosity and a slower decrease in transmissivity with depth (deep layer average porosity of 0.40 compared to 0.53 in Model B and 0.54 in Model C). Model B is notable for having relatively deep soil (3.8 m average compared to 2.8 m in Model A and 2.4 m in Model C). Model C is notable for having relatively low transpiration rates (average minimum stomatal resistance across conifer classes of 260 s/m compared to 189 s/m in Model A and 187 s/m in Model B). All three selected models have relatively high effective hydraulic conductivities, near the 95th percentile of the POLARIS data (Chaney et al., 2019), with snow parameters converging reasonably close to those estimated by Sun et al. (2019) for the Sierra Nevada region.

The ensemble of calibrated DHSVM models reproduces key hydrological signatures during historic calibration and validation periods. During the calibration period (water years 2012–2017), the three selected models achieve a mean area-weighted daily NSE of 0.82 across all 10 gauged watersheds, with an area-weighted NSE of 0.75 indicating a moderate decrease in skill on the validation period (water years 2006–2011). The decrease in NSE during the validation period could be caused in part by lower year-to-year variability in streamflow, which reduces the total sum of squares (denominator of NSE). In the North Yuba watershed (USGS station 11413000), which is the largest gauged basin without upstream flow regulation in our study area (650 km^2), the calibrated models produce a mean daily NSE of 0.87 over the calibration period and 0.80 over the validation period (Figure 3). In log-transformed space, the calibrated models produce calibration and validation NSEs of 0.94 and 0.92 in the North Yuba. DHSVM satisfactorily reproduces both low-flow and high-flow regimes at this gauge, including major peak

flows associated with rain-on-snow events in the winter of 2017 (Figure 3). Daily NSEs are more variable in smaller watersheds (11–130 km^2), typically in the range of 0.6–0.8 for both calibration and validation periods with occasional larger errors associated with incorrect rain-snow partitioning at the ~10 km^2 scale in steep terrain (refer to Supporting Information S1 for a full set of hydrographs).

At full watershed scales, DHSVM shows low bias in water yield, with bulk runoff errors of −8% to +2% at the YRS and AMF full natural flow points during calibration and validation periods (mean error −3% across all models and periods at both measurement points). The calibrated models also satisfactorily reproduce variability in large-scale peak flows, interannual variability in pixel-wise maximum yearly SWE, and interannual variability in pixel-wise maximum yearly SWE timing (Figures S4–S13 in Supporting Information S1). On the 6-year validation period, basin-average mean ET from the Yuba and American basins is 742 or 655 mm/yr, with an interannual range of 613–832 mm/yr or 542–750 mm/yr, respectively. These DHSVM-simulated ET estimates are reasonably close to empirical estimates of 675 ± 57 or 619 ± 54 mm/yr in the Yuba and American, respectively, based on eddy covariance data and normalized difference vegetation index (NDVI) extrapolation (Roche et al., 2020).

3.2. Forest Ecosystem Response to Disturbance

The LANDIS-II forest ecosystem model produces spatially explicit timeseries of vegetation characteristics across a spectrum of prescribed forest management scenarios. Conifer forests cover most of our central Sierra Nevada study region with the exception of high alpine regions and lakes, most notably Lake Tahoe. The historical baseline map from LANDIS-II, used for DHSVM calibration, has an area-averaged grid cell LAI of 2.3 m^2/m^2, with a median of 2.2 m^2/m^2 and a 90th percentile of 4.5 m^2/m^2. The densest forests are historically concentrated at mid-elevations on the west slope of the mountain range (Figure 2c).

Partial or full restoration of the historic forest disturbance return interval produces relatively thinner forests. Regardless of management scenario, LANDIS-II indicates a substantial decrease in forest density by the end of the century primarily from increased insect mortality (Maxwell et al., 2022). In the business-as-usual scenario (S2), LANDIS-II shows a mean LAI of 1.5 m^2/m^2 at the end of the century (median 1.3 m^2/m^2 and 90th percentile 3.4 m^2/m^2), which is a decrease of 33% relative to the 2015 mean (averaged across both climate projections). Comparatively, the reduced treatment scenario (S1) shows a 32% decrease in mean LAI, the partial disturbance scenarios show a 36% decrease in mean LAI (both S3 and S4), and the full disturbance scenarios show a 43% (S5, less fire) or 47% (S6, more fire) decrease in mean LAI over the same 85-year period. All scenarios produce LAI distributions with mean values that are mutually separable at $p < 10^{-15}$, except S3 and S4, which are separable at $p < 0.05$ (Welch two sample t-test). At the end of the century, mean LAI in the full disturbance scenario (S6) is 0.31 m^2/m^2 lower (−20%) compared to the business-as-usual scenario (S2). Scenario differences in end-of-century LAI are largest in the same mid-elevation west slope regions that have the densest initial forest cover (Figures 2c and 2d), up to a maximum sub-watershed difference of 1.2 m^2/m^2 (39%) between full disturbance and business-as-usual scenarios. The spatial distribution of LAI becomes relatively more homogeneous over time (at the landscape scale) because areas with high initial LAI have the most forest stock available for reduction. In all scenarios and both climates, LANDIS-II predicts significant species changes during the 85-year simulation period; most notably, white fir (A. concolor) cover substantially decreases and Douglas fir (P. menziesii) cover increases. Additionally, understory cover increases at higher elevations regardless of management scenario. Refer to Figure S14 in Supporting Information S1 for maps of initial and final vegetation types and understory LAI and Figure S15 in Supporting Information S1 for the time evolution of overstory LAI.

3.3. Simulated Effects on the Snowpack

In management scenarios with a relatively thinner forest canopy, DHSVM predicts relatively higher landscape-average snowpack accumulation. A pixel-wise average of the peak yearly SWE in all three models and all 85 years provides a spatial metric for snow accumulation during the simulation period (Figure 4). Compared to business-as-usual (S2), the mean pixel-wise peak SWE in the full disturbance scenario (S6) is about 5% higher in the wetter CNRM-CM5 climate and about 6% higher in the drier MIROC5 climate ($p < 10^{-15}$). In both climates, the absolute magnitude of peak SWE differences between S6 and S2 varies between about −5 and +12 cm (1st and 99th percentiles). The spatial heterogeneity of SWE accumulation effects is only slightly lower (−4 to +13 cm) when only considering grid cells where LAI is lower in S6 than S2 to account for the effect of stochastic

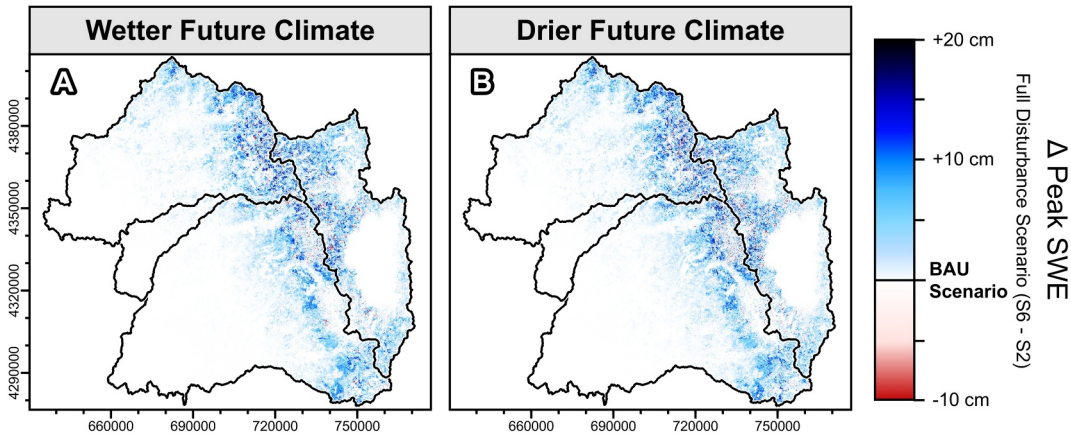

Figure 4. Difference in pixel-wise peak snow water equivalent (SWE) between the full disturbance (S6) and business-as-usual (BAU, S2) forest management scenarios, calculated as an average over the full 85-year period under the CNRM-CM5 (wetter) and MIROC5 (drier) RCP 8.5 climate projections.

disturbance locations in LANDIS-II outputs. Thus, most of the modeled heterogeneity in the snowpack response to forest thinning (Figure 4) is attributable to meaningful differences in the model response to spatial variability rather than merely spatial noise resulting from the stochasticity of the prescribed treatments. Due to the large number of model grid cells ($N \sim 10^6$), there are significant ($p < 10^{-15}$) Pearson correlations between the peak SWE change and numerous topographic and environmental metrics, including northness, eastness, elevation, LAI, and LAI change, but only elevation ($r = -0.40$) and LAI change ($r = -0.13$) have correlations with magnitude >0.1. This suggests that spatial variability in the simulated snowpack response to forest disturbance arises due to interactions between multiple variables and/or nonlinear relationships with the tested variables. Note that all statistical test results related to DHSVM results are estimated from spatiotemporal variability in the model response, and in a strict sense, any difference between model outputs is equally significant with a deterministic model like DHSVM.

We observe that the percent change in pixel-wise peak SWE is relatively consistent throughout the simulation period, but the effect begins to attenuate during the 2070s–2090s as precipitation increasingly falls as rain in a warmer future climate (Figure S16 in Supporting Information S1). Over the full 85-year simulation period, 15% of total precipitation falls as snow in the CNRM-CM5 climate, and 18% in MIROC5. Considering just the latter half-century (2050–2099), those percentages decrease to 11% and 16%, respectively. The pixel-wise snow ablation rate, calculated from the peak SWE date to the melt-out date, increases by around 1%–10% in most years, except late in the century when thinner forests melt out marginally slower (Figure S17 in Supporting Information S1).

3.4. Simulated Effects on Streamflow Generation

DHSVM predicts an increase in streamflow generation from forested sub-watersheds in the central Sierra Nevada with an increased pace of forest disturbance (Figure 5). On average over the 85-year simulation period across the whole study area and all three models, DHSVM predicts 4.3% more total streamflow generation in S6 relative to S2 under the wetter CNRM-CM5 climate, and 5.7% more total streamflow generation under the drier MIROC5 climate. However, the effect of forest disturbance on local streamflow generation is heterogeneous in space and time. In certain sub-watersheds, the average 85-year streamflow change is as high as +27% in the drier climate and +22% in the wetter climate. Conversely, the effect is near zero in sub-watersheds with low initial forest cover. Decreases in streamflow generation (as low as −4%) are observed where forest cover is locally denser in S6 than in S2, a result of stochasticity in the spatial distribution of fires between different LANDIS-II runs. Averaging over only the driest 10 years in each climate projection, sub-watershed streamflow generation increases by up to +35% under the drier MIROC5 climate (median = +6%, 90th percentile = +18%, mean >0 at $p < 10^{-15}$ using one-sample *t*-test) and up to +27% in the wetter CNRM-CM5 climate (median = +7%, 90th percentile = +18%, mean >0 at $p < 10^{-15}$). In summary, restoring a more frequent disturbance return interval to Sierra Nevada forests has the greatest relative effect on streamflow generation during dry years and where pre-disturbance forests are especially dense.

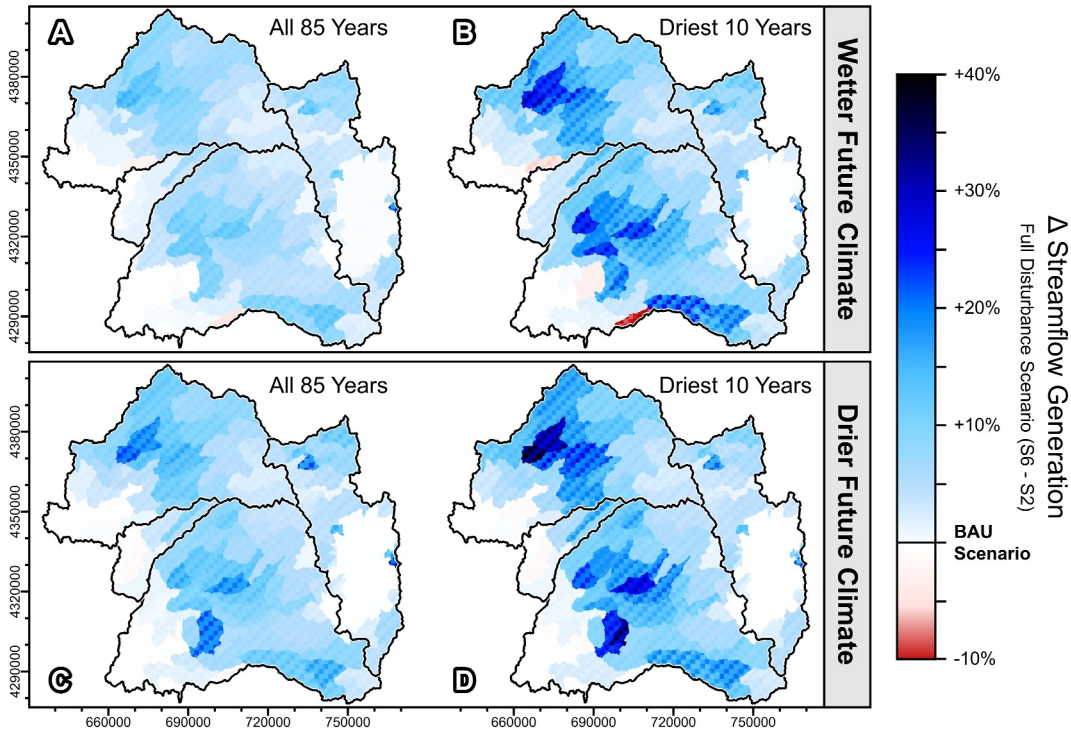

Figure 5. Percent difference in local streamflow generation for 139 sub-watersheds in the full-disturbance (S6) forest management scenario relative to the business-as-usual (BAU, S2) scenario, calculated as an average over the full 85-year period (a, c) and as an average over the driest 10 years in each climate (b, d). The checkerboard pattern is produced by interweaving results from three calibrated Distributed Hydrology Soil Vegetation Model models, representing hydrological model uncertainty.

Sub-watersheds show significantly different streamflow generation responses depending on the local climate and initial forest conditions. The absolute streamflow generation response to forest disturbance (S6–S2) in units of water depth (Figure S18 in Supporting Information S1) has a median of 45 mm/yr or 39 mm/yr, a 90th percentile of 93 mm/yr or 82 mm/yr, and a maximum of 151 mm/yr or 142 mm/yr in the wetter (CNRM-CM5) and drier (MIROC5) climates, respectively (mean sub-watershed change >0 at the $p < 10^{-15}$ level for both climates). Spatial heterogeneity in the absolute (not percentage) effect on streamflow generation correlates with the sub-watershed mean historical LAI (Pearson correlation $r = 0.69$), the LAI difference between scenarios at the end of the century ($r = 0.93$), and precipitation ($r = 0.64$), with only a weak correlation to elevation ($r = 0.14$). All correlations are significant at the $p < 10^{-15}$ level except for elevation, which is significant at $p < 0.05$ although the correlation is weak.

Comparing Figures 2 and 5, we note that the largest percentage gains in streamflow occur in watersheds at low-to mid-elevations on the west slope of the Sierra Nevada where the forest is initially dense and precipitation is relatively low. In this relatively arid zone, pre-disturbance streamflow generation is low, so small changes to the water balance can lead to large percentage streamflow gains. Considering absolute differences in area-normalized streamflow instead of percentage differences, forest disturbance has the largest effect in sub-watersheds with a combination of relatively high precipitation and dense pre-disturbance forests. There is considerable overlap between sub-watersheds with large percent increases and large absolute increases ($r = 0.74$, $p < 10^{-15}$). However, the largest percentage increase (+27%) is predicted in a sub-watershed with only a 40th percentile absolute increase (30 mm/yr). Most of the landscape-scale increase in water yield is attributable to forest disturbance in relatively wet regions, but the largest relative impacts on streamflow generation occur in relatively dry regions.

3.5. Simulated Effects on Water Balance Partitioning

Precipitation inputs to DHSVM are identical in all management scenarios, so changes in other water balance terms must sum to zero. Calculating the difference in water balance fluxes between forest management scenarios

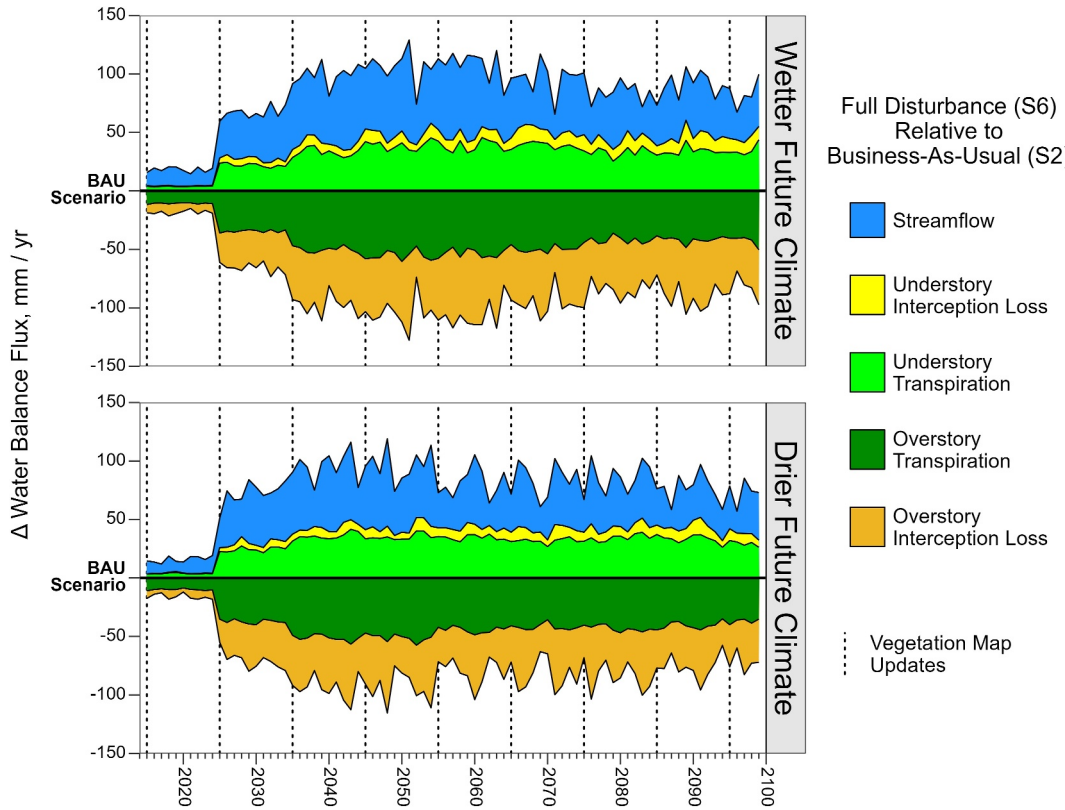

Figure 6. Timeseries of differences in yearly water balance fluxes between full disturbance (S6) and business-as-usual (BAU, S2) forest management scenarios, averaged across the entire study area. All terms are calculated as the difference between forest management scenarios with equal precipitation, so all changes in the water balance fluxes visualized here approximately sum to zero each year. Fluxes that are larger component of the water balance in S6 relative to S2 are positive here, and vice versa. Dashed vertical lines indicate dates where vegetation maps in Distributed Hydrology Soil Vegetation Model are updated using outputs from LANDIS-II.

reveals the impact of forest disturbance on water balance partitioning. Yearly storage changes and soil evaporation only show negligible differences between management scenarios, so these terms are excluded from comparison here. The negligible change in simulated soil evaporation is partially a result of our assumption that light understory is present in all forested grid cells (Section 2.1). In other DHSVM simulations without uniform understory, we have observed a similar compensating effect between overstory ET and bare soil evaporation. Thus, the increase in understory ET reported here could substitute for increases in soil evaporation in areas that might not meet our assumption of understory coverage.

Systematic increases in water yield from forest disturbance are primarily attributable to decreased canopy interception loss, because increases in understory transpiration largely compensate for decreases in overstory transpiration (Figure 6). For the remainder of this section, analogous numeric values are given first for the wetter future climate (CNRM-CM5) and second for the drier future climate (MIROC5). Mean overstory transpiration is 42 or 40 mm/yr lower on average across all years in the full disturbance scenario relative to business-as-usual. However, mean annual understory transpiration is 31 or 29 mm/yr higher in the full disturbance scenario, which compensates for 72% or 73% of the reduction in overstory transpiration. Mean interception loss from the canopy is 41 or 35 mm/yr lower in the full disturbance scenario, while understory interception loss increases by only 9 or 7 mm/yr, a smaller compensation of 21% in both climates. Since increases in understory ET do not fully compensate for decreases in overstory ET, the full disturbance scenario generates 45 or 40 mm/yr more streamflow on average relative to the business-as-usual scenario. About 27% or 28% of the increased streamflow generation in the full disturbance scenario is attributable to decreased transpiration and about 73% or 72% of increased streamflow generation is attributable to decreased interception loss. All of these flux changes are significant at the $p < 10^{-15}$ level considering variability across all water years, models, and climates. Similar

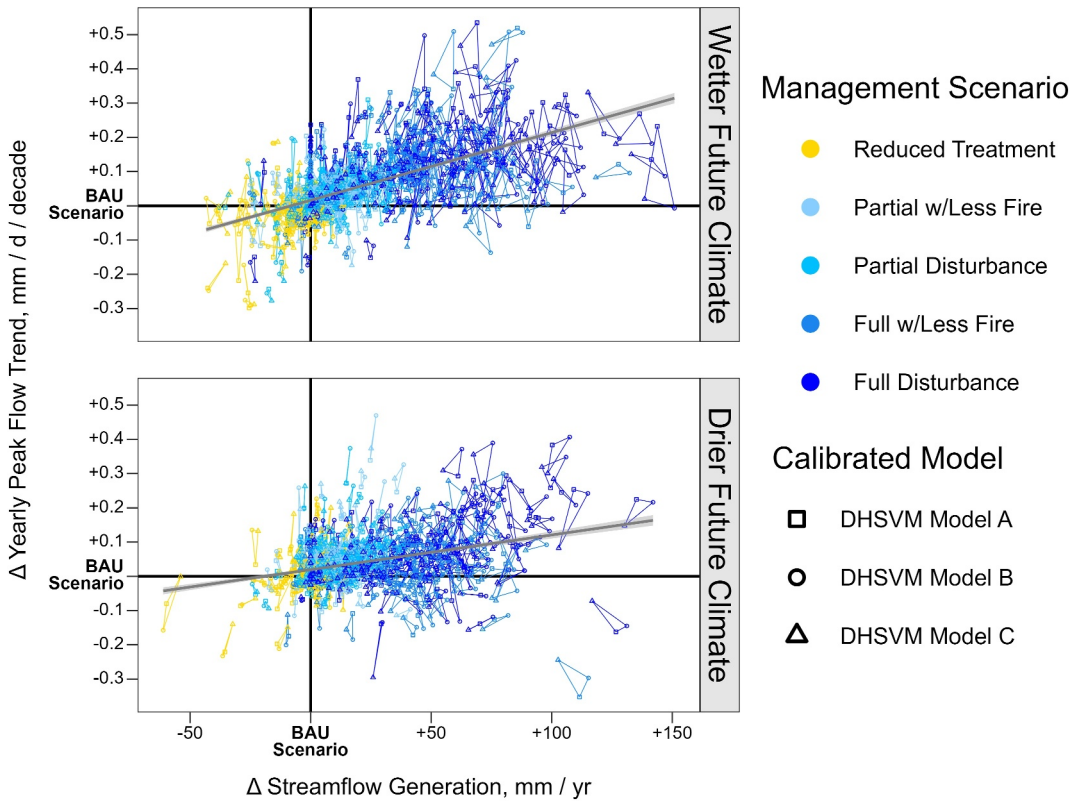

Figure 7. Relationship between increased streamflow generation and increased one-day yearly peak flows for sub-watersheds subject to different forest management scenarios. Differences in streamflow generation and peak flow trend are shown for each scenario relative to the business-as-usual (BAU, S2) scenario. Each point represents a single sub-watershed simulated with a particular Distributed Hydrology Soil Vegetation Model (DHSVM) model. The results from all three calibrated DHSVM models are connected with line segments, creating a triangular region that represents uncertainty in the response of each sub-watershed.

albeit much smaller changes in the water balance partitioning are expected with partial restoration of the disturbance interval (Figure S26 in Supporting Information S1).

3.6. Simulated Effects on Peak Flows

DHSVM predicts a trend toward relatively higher one-day yearly peak flows in sub-watersheds that are subject to a relatively frequent forest disturbance regime. Both the CNRM-CM5 and MIROC5 climate projections cause trends toward higher peak flows in 95% of the 139 sub-watersheds in the project area ($p < 10^{-15}$), calculated as the Sen's slope of one-day yearly peak flows. The peak flow trend is stronger in the relatively wet CNRM-CM5 climate, with a median sub-watershed peak flow trend of +7.5% per decade in the business-as-usual management scenario. The analogous median trend in the drier MIROC5 climate is +3.3% per decade. In both climates, scenarios with a more frequent forest disturbance return interval can produce hydrographs with accelerated peak flow trends in certain sub-watersheds (Figure S19 in Supporting Information S1). Relative to business-as-usual (S2), yearly one-day peak flows in the full disturbance scenario (S6) are 3% or 6% higher ($p < 10^{-15}$) on average across all sub-watersheds in the wetter and drier climates, respectively. There is a large degree of variation in the relative sub-watershed peak flow response (Figure S20 in Supporting Information S1), and the maximum difference between mean annual peak flows for particular sub-watersheds in these two scenarios is as high as 23% in the wetter climate or 39% in the drier climate. However, percentage-based metrics can overemphasize sub-watersheds with relatively low streamflow, since a small increase is a larger fractional change. It is more informative to compare Sen's slope decadal trends in area-normalized specific discharge units (mm/d/decade), as in Figure 7. Note that the streamflow generation effect is calculated after subtracting upstream watershed contributions, but the peak flow trend is calculated from raw hydrographs to represent the actual peak flows in a particular channel reach (including upstream contributions).

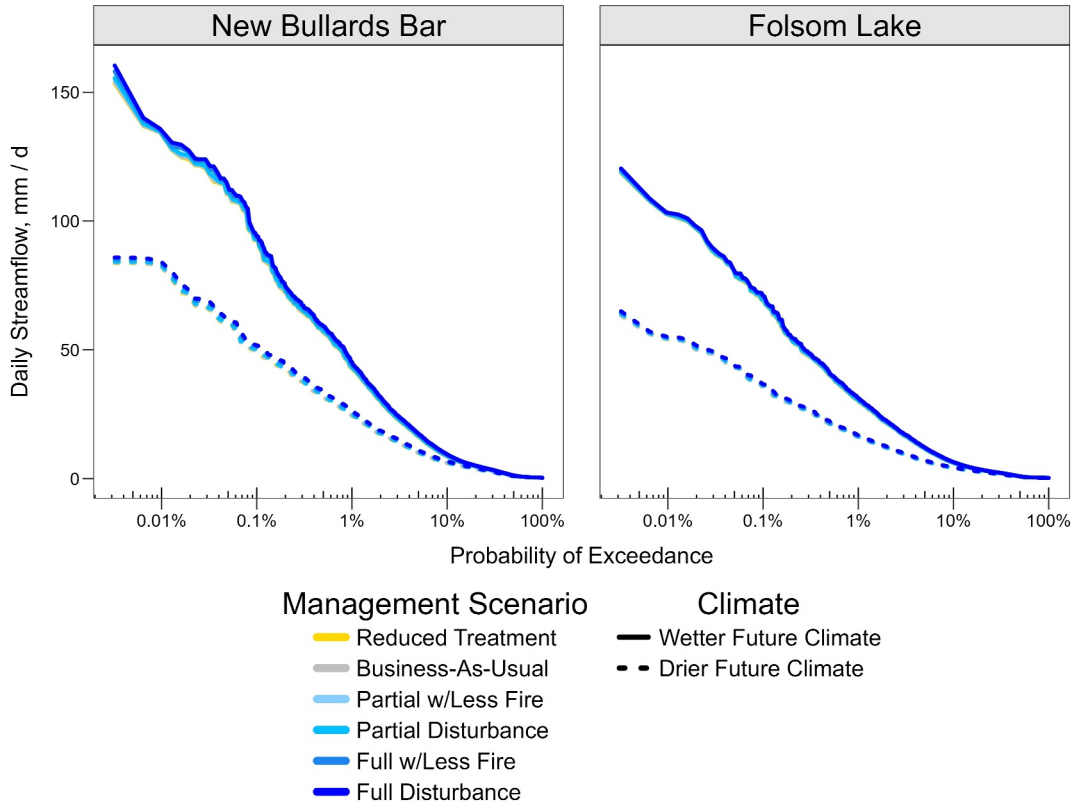

Figure 8. Flow duration curves for two major reservoirs in the project area, calculated using daily natural (unregulated) inflows simulated by Distributed Hydrology Soil Vegetation Model for the full 85-year period. Note the large difference in the high flow regime between climate models compared to the small difference in high flows between forest disturbance scenarios. The probability of exceedance is logarithmically scaled to emphasize variations in the high flow regime.

We observe a tradeoff between increased streamflow generation and elevated peak flow trends in scenarios with relatively more frequent forest disturbance (Figure 7). Considering all sub-watersheds across all management scenarios, the correlation between additional water yield and a higher peak flow trend is stronger in the wetter future climate ($r = 0.60$ in CNRM-CM5 and $r = 0.33$ in MIROC5, $p < 10^{-15}$ for both). Relative to the business-as-usual scenario (S2) and averaged across all three models, both climates, and all 139 sub-watersheds (area-weighted), the reduced treatment scenario (S1) has 2 mm/yr less streamflow generation and no clear pattern of peak flow change. The scenarios with partial restoration of the disturbance return interval have increased streamflow generation of 8 mm/yr (S3, less fire) or 9 mm/yr (S4, more fire), with peak flow trends higher by 0.036 mm/d/decade (S3) or 0.037 mm/d/decade (S4). Finally, full restoration of the disturbance return interval produces increased streamflow generation of 34 mm/yr (S5, less fire) or 42 mm/yr (S6, more fire), with peak flow trends higher by 0.062 mm/d/decade (S5) or 0.094 mm/d/decade (S6). Compared to the partial disturbance scenarios (S3 and S4), the full disturbance scenarios (S5 and S6) are about 4.5 times as efficacious at producing additional streamflow. At the same time, sub-watershed mean annual peak flows in the full disturbance scenarios are about 3% higher than in the partial disturbance scenarios.

At watershed scales that are relevant for reservoir operations, the effect of forest disturbance on peak flows is overwhelmed by the uncertainty of future climate projections. There are two major artificial reservoirs in the project domain: New Bullards Bar (capacity 966,00 acre-ft./1.19 km^3) in the North Yuba River watershed, and Folsom Lake (capacity 976,000 acre-ft./1.20 km^3) at the outlet of the American River watershed. Comparing daily flow duration curves for both of these reservoirs derived from DHSVM shows that forest management only has potential to exert a negligible impact on the high flow regime compared to the uncertainty in future precipitation trends (Figure 8). We note that the reservoir-scale peak flow statistics presented here are calculated from raw modeled hydrographs, not accounting for upstream diversions or artificial storage, and are thus not suitable for direct comparison with historical flow records. Over all 85 years in the simulation period, the

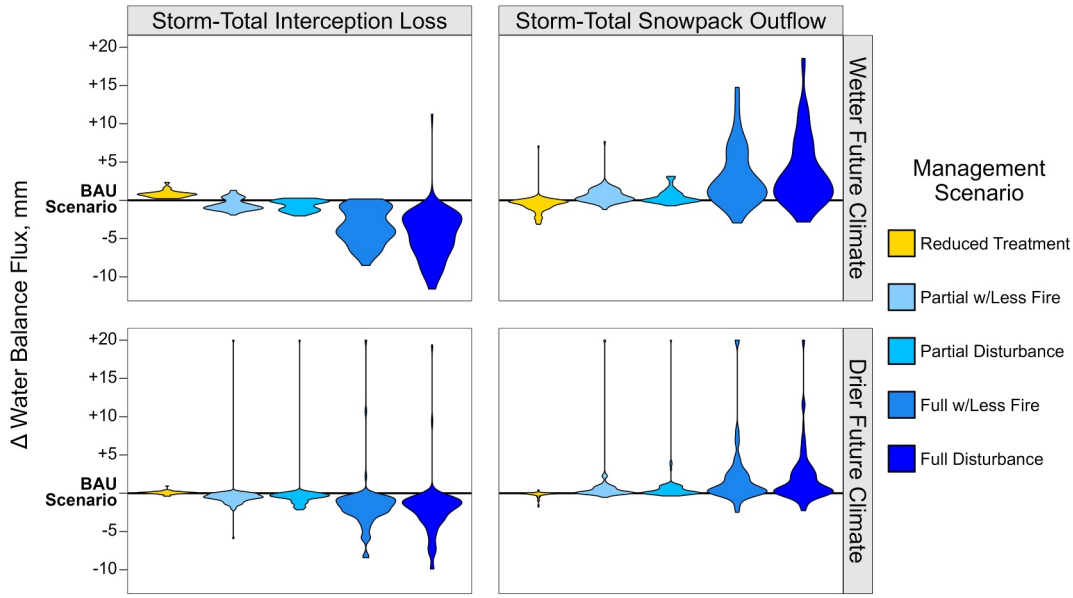

Figure 9. Forest disturbance effect on storm-total interception storage, storm-total cumulative interception loss, and storm-total snowpack outflow during intense precipitation events prior to yearly peak flows, calculated as a landscape average for each of four major watersheds simulated by each of three Distributed Hydrology Soil Vegetation Model models. Results are shown for the full-disturbance scenario (S6) relative to the business-as-usual (BAU, S2) scenario.

mean yearly one-day peak flow is 80% higher for New Bullards Bar and 94% higher for Folsom Lake in CNRM-CM5 compared to MIROC5. Comparing the same statistic between full disturbance (S6) and business-as-usual (S2) scenarios, the mean yearly one-day peak flow increases by 4% or 7% for New Bullards Bar and 4% or 6% for Folsom Lake in the CNRM-CM5 and MIROC5 climates, respectively. Thus, uncertainty in the future climate is about 14 times or 20 times larger than the potential impact of forest thinning on annual peak flows into New Bullards Bar and Folsom Lake, respectively.

3.7. Simulated Effects on Hydrological Processes During Major Storms

In scenarios with a thinner forest canopy, decreased interception and increased snowmelt can both contribute to increased runoff during major storms (Figure 9). As discussed in Section 2.3, we define the 10 highest-intensity storms (cross-storm average of 66 mm/d, 404 mm storm-total precipitation) immediately preceding yearly peak flow events in each of the four main watersheds for all three DHSVM models, thus identifying 120 storm runoff simulations in each scenario for each climate projection. In the full disturbance scenario relative to business-as-usual, interception loss (evaporation and sublimation) is generally decreased (mean −3.5 mm during storm, $p < 10^{-15}$) while snowpack outflow is generally increased (mean 3.8 mm during storm, $p < 10^{-4}$) during these storm runoff periods. Some combinations of watershed and hydrological model produce outlying results for certain storms: S6 versus S2 simulated differences are non-conforming with respect to the mean in 2% of cases for interception loss and 11% of cases for snowpack outflow. In our simulations, forest disturbance has a much larger effect on cumulative storm-total interception vapor loss compared to net storm-total interception storage, because the same storage capacity may be filled and evaporated repeatedly during multi-day storms. Only 8% of precipitation falls as snow during the selected highest-intensity storm events. Snowpack outflow from DHSVM includes both snowmelt and rain percolation, so some or all of the increased snowpack outflow in scenarios with a thinner canopy may be attributable to increased rain throughfall caused by reduced canopy interception.

During storm events associated with yearly peak flows, the effect of a thinner forest canopy on the snowpack energy balance varies in space and time. Compared to business-as-usual, in the full disturbance scenario the snowpack generally receives increased shortwave radiation, increased advected energy (from precipitation throughfall), and decreased longwave radiation (Figure 10). In the full disturbance scenario, these effects each have mean tendencies that are significant at $p < 10^{-5}$. However, as a result of differing positive or negative changes to shortwave, longwave, and advected energy, the net snowpack energy budget in a thinner forest may

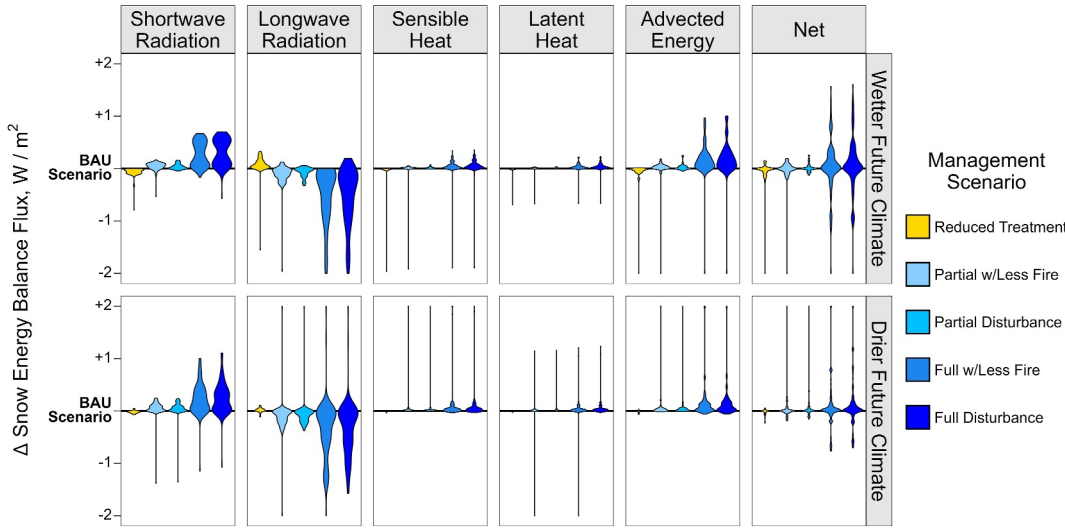

Figure 10. Forest disturbance effects on the landscape-average snowpack energy balance during major precipitation events prior to yearly peak flow events in each of four major watersheds simulated by each of three Distributed Hydrology Soil Vegetation Model models relative to the business-as-usual scenario.

increase or decrease depending on the specific circumstances of each storm, with an insignificant mean change at the $p < 0.1$ level. Simulated sensible and latent heat fluxes show only very small changes. We note that the small magnitude of energy balance changes in Figure 10 (on the order of 1 W/m^2) are area-averaged values for the entire TCSI area, while snow only exists in limited areas during these storm events, especially in later decades. Thus, Figure 10 quantifies relative patterns of change but does not represent the absolute magnitude of changes to the snowpack energy balance.

3.8. Uncertainty in Sub-Watershed Streamflow Responses

The uncertainty of the calibrated hydrological model (DHSVM) is considerably smaller than both the average magnitude and spatial heterogeneity of the predicted streamflow generation effects, though climate uncertainty is nevertheless substantial. In Figure 5, which shows the additional streamflow generation attributable to forest disturbance, analogous results from all three selected DHSVM models are interwoven using a checkerboard pattern, where every third square is representative of the value from a single calibrated model. The resolution of the checkerboard is selected for ease of visualization, and the actual grid size of DHSVM is much smaller (90 m). Greater uniformity in the checkerboard pattern indicates proportionally lower uncertainty in the hydrological model ensemble. Overall, the uncertainty between different DHSVM ensemble members is about an order of magnitude smaller than the size of the predicted effects attributable to forest management.

The peak flow response to forest thinning is more uncertain than the streamflow generation response, but both responses show significant patterns of spatial heterogeneity. In Figure 6, hydrological model uncertainty is visualized with triangles defined by the results from all three calibrated DHSVM models in each sub-watershed. Although the true response of a given sub-watershed could fall outside the bounds of its modeled range (enclosed triangle), the overall spread of the three ensemble members gives an estimate of model uncertainty. In the full disturbance (S6) scenario relative to business-as-usual (S2), the sub-watershed streamflow generation response has an average model uncertainty range of 5.3 mm/yr among the three DHSVM models and an average difference of 7.9 mm/yr between both climate models. The mean sub-watershed streamflow response to forest disturbance (S6 vs. S2) is 44 mm/yr with a standard deviation among sub-watersheds of 32 mm/yr. Analogously, the S6 versus S2 peak flow trend difference in each sub-watershed varies by 0.075 mm/d/decade on average among DHSVM models and 0.090 mm/d/decade on average between climates, with a mean across sub-watersheds of 0.097 mm/d/decade and a standard deviation among sub-watersheds of 0.083 mm/d/decade. For most sub-watersheds, the magnitude of the predicted streamflow generation response considerably outweighs both the uncertainty of the model (~12%) and the mediating effect of climate (~18%), but the peak flow response has much higher model uncertainty (~78%) and much greater dependence on climate mediation (~93%).

Nevertheless, we observe that the largest sub-watershed peak flow responses are relatively well-constrained based on the individual confidence regions in Figure 6. The maximum response for any one sub-watershed averaged across models and climates is 140 mm/yr of additional streamflow generation or a 0.37 mm/d/decade higher peak flow trend. Thus, locally strong sub-watershed responses are well-resolved relative to the model uncertainty.

3.9. Uncertainty in Reservoir-Scale Water Yield

Despite uncertainty in the future climate, the absolute magnitude of additional water yield into reservoirs under different forest disturbance scenarios is well-constrained. Here, we consider mean yearly runoff into each reservoir over the full 85-year simulation period in the full disturbance scenario (S6) relative to the business-as-usual scenario (S2). For the New Bullards Bar watershed, DHSVM predicts an additional 99,800 acre-ft/yr (0.123 km^3) of yearly runoff in the wetter CNRM-CM5 climate or an additional 90,700 acre-ft/yr (0.112 km^3) of yearly runoff in the drier MIROC5 climate. For Folsom Lake, the additional inflow is 176,000 acre-ft/yr (0.217 km^3) under CNRM-CM5 or 158,000 acre-ft/yr (0.195 km^3) under MIROC5. The total mean annual runoff between wetter and drier climate projections varies by 46% for New Bullards Bar and 55% for Folsom Lake, but the volume of additional runoff attributable to forest disturbance varies by only 10% or 12% between climates for the same reservoirs. Thus, the additional water yield from forest disturbance is about five times less sensitive to uncertainty in future precipitation trends compared to the total future water yield (46% vs. 10% uncertainty for New Bullards Bar and 55% vs. 12% uncertainty for Folsom Lake).

The relative contribution of additional runoff from forest disturbance as a percentage of the total yearly volume is dependent on future climate trends and interannual variability. Relative to the business-as-usual scenario, additional water yield from the full disturbance scenario amounts to 7% or 9% of the mean annual inflow for New Bullards Bar and 4% or 6% for Folsom Lake in the wetter or drier climate projections, respectively. Considering only the 10 driest years (by annual precipitation), the absolute additional runoff in the full disturbance scenario relative to business-as-usual is 71,900 acre-ft/yr (0.0887 km^3) or 52,300 acre-ft/yr (0.0645 km^3) for New Bullards Bar and 113,000 acre-ft/yr (0.139 km^3) or 78,400 acre-ft/yr (0.0967 km^3) for Folsom Lake in the wetter and drier climate projections, respectively. This additional runoff amounts to 12% or 14% of the total annual inflow for New Bullards Bar and 8% or 9% of the total annual inflow for Folsom Lake during the same 10 driest years, again in the wetter or drier climates. While the absolute volume of additional water yield attributable to forest disturbance decreases during dry climate conditions, the percent difference between business-as-usual and full disturbance scenarios increases. Therefore, restoring the historic disturbance return interval would have the largest relative impact on reservoir-scale water yield during drought years, particularly in a drier climate.

4. Discussion

4.1. Reservoir-Scale Drought Hedge

Our results suggest that increased water yields from landscape-scale restoration of more frequent forest disturbance can provide a hedge against future droughts in the central Sierra Nevada region, on the order of 8%–14% increases in reservoir water yield during dry years. Compared to the annual water yield, streamflow gains from increased forest disturbance are about five times less sensitive to uncertainty in the annual precipitation volume. This reduced sensitivity of streamflow gains follows from the partial decoupling of precipitation and forest ET in the relatively energy-limited study region, as previously shown by Saksa et al. (2017) for the same geographic area. This result is hydrologically intuitive because the impact of forest thinning is bounded by the maximum interception loss and transpiration rates supported by the initial forest. For example, trees have a minimum stomatal resistance beyond which additional soil moisture does not increase transpiration rates. Similarly, once interception storage becomes saturated during a storm, additional precipitation is less affected by canopy structure. From a management perspective, the environmental and economic value of additional streamflow generated from a thinner forest is likely to be contingent upon trends in future precipitation (see Guo et al., 2023 for a discussion of the marginal price of water in the study region). Even in a wetter future climate, certain years will likely still qualify as droughts, and the partial decoupling of additional runoff from precipitation could benefit the water supply in those dry years. Thus, the value proposition of restoring the historic disturbance interval for water resources in the central Sierra Nevada region may best be understood as a hedge against a possible drier future climate and/or drought years in any future climate.

The magnitude of additional water yield from forest disturbance as predicted by DHSVM is generally supported by prior findings in similar environments. In a small sub-basin of the American River watershed, included in our study area, Saksa et al. (2017) used a combination of process-based modeling and field data to estimate a 14% increase in streamflow generation after forest thinning. While a direct comparison is not possible due to differences in scale and treatment intensity, the empirical findings of Saksa et al. (2017) align with our model results in the same geographic region (Figure 5). Using statistical approaches based on relationships between measured ET and maps of the NDVI from remote sensing, Roche et al. (2020) estimate a 150–200 mm/yr potential streamflow gain from forest fires or thinning in the American and Yuba River watersheds. This streamflow gain is larger than predicted by our simulation for almost all sub-watersheds (Figure 7). While individual fires might cause extreme changes in the local water balance, our results indicate that it would be overly optimistic to expect such a large streamflow response from forest disturbance at the landscape or even sub-watershed scale. Similarly, Guo et al. (2023) estimate reductions in ET as high as 361–371 mm/yr for high-severity wildfire or 269–277 mm/yr for medium-severity wildfire for small forest treatment areas (15.6–23.1 km^2) at the headwaters of the Yuba and American watersheds. Our results similarly suggest that these high ET reductions are unlikely to be realized from forest disturbance at larger landscape scales, and we estimate a mean landscape ET reduction (overstory and understory transpiration plus interception loss) of only 41 mm/yr in the full disturbance scenario. Nevertheless, extrapolation of empirical NDVI-based methods can produce similar water yield results at the landscape scale, provided that enough recent fires have occurred in the region of interest to constrain variable vegetation responses to disturbance. In the American River watershed, Roche et al. (2018) estimate a 5% (all years) or 10% (dry years) increase in reservoir inflow under a restored disturbance regime, remarkably close to the increase of 4%–6% (all years) and 8%–9% (10 driest years) modeled for the same basin in this study.

4.2. Sub-Watershed Heterogeneity

The additional water yield from forest disturbance could be maximized by targeting treatments to sub-watersheds with particularly dense forests and high average precipitation. Forest management planning could prioritize mechanical thinning and prescribed fire in sub-watersheds with the greatest potential for increased streamflow generation (Figure 5). Additionally, a machine learning model such as Random Forest could potentially be trained on the process-based DHSVM results in a meta-model decision support framework (Mijic et al., 2024), such as the tool implemented by Lewis et al. (2023) for the snowpack response to forest disturbance in the same geographical region. Other studies have demonstrated the ranges of forest density and canopy gap size that can best promote snow accumulation (Piske et al., 2024), but these fine scales are not explored in the present study. With knowledge of the potential tradeoff between increased streamflow generation and higher peak flow trends (Figure 7), it may be desirable to target forest disturbance in sub-watersheds that balance the utility of additional water yield against the risk of damage to small-scale infrastructure from high flows. In the TCSI region, the elevation head and capacity of downstream hydroelectric plants further mediates the potential benefit of additional streamflow generation (Guo et al., 2023). From a water resources perspective, the ideal areas for forest disturbance could be dense forests that are situated above power-generating reservoirs, since these reservoirs can benefit from increased inflow and mediate increases in peak flows.

Although forest disturbance may cause locally higher peak flows, any significant impacts are limited to headwaters and are unlikely to affect reservoir operations. DHSVM predicts peak flow increases on the order of 10%–30% in certain sub-watersheds, but these are small headwaters catchments with relatively low absolute streamflow magnitudes, on the order of 0.1–10 m^3/s (Figure S21 in Supporting Information S1). Increases in small-scale peak flows could accentuate risks to hydraulic infrastructure such as road culverts, many of which are only engineered for 25-year peak flows and are now aging and vulnerable to washouts (Halofsky et al., 2021). Additionally, elevated surface runoff in headwaters regions could exacerbate erosion and sediment loading from historic hydraulic mining sites, which are prevalent in the study area (Curtis et al., 2005; Gilbert, 1917). The effect of forest disturbance on peak flows attenuates rapidly at larger scales, and reservoir operations are unlikely to be significantly impacted by landscape-scale forest disturbance in the central Sierra Nevada region. One key uncertainty in our results is the lack of changes in the DHSVM soil and snow properties that could contribute to faster runoff or faster snowmelt, such as increased soil hydrophobicity (Certini, 2005) or darkened snow albedo from pyrogenic carbon (e.g., Gleason et al., 2013, 2019). Because uncertain future precipitation trends almost exclusively control the high flow regime, flood management planning will likely become increasingly motivated by the potential for extreme precipitation and rapid snowmelt events (Harpold & Kohler, 2017; Hou et al., 2019).

For example, a project is currently planned to add a second spillway to the New Bullards Bar Reservoir to reduce flood risk associated with atmospheric river storms (Yuba Water Agency, 2023).

4.3. Overstory-Understory Compensation

A process-based modeling approach is necessary to untangle the compensating responses of overstory and understory vegetation to forest disturbance. Reduced canopy interception can lead to greater terrestrial water input (rain + snowmelt), and lower overstory transpiration can lead to higher soil moisture. Not all excess terrestrial water input necessarily becomes streamflow though, as noted empirically after widespread insect-driven forest mortality (e.g., Biederman et al., 2015). Wetter soil and reduced canopy shading can both contribute to increases in ET from remaining vegetation and soil evaporation (Boisramé et al., 2019). Moreover, elevated soil moisture may encourage regrowth of both understory and trees, so continued treatment by mechanical thinning or fire is necessary to maintain a thinner forest state, as implemented in the scenarios tested here (Maxwell et al., 2022). Similarly to the findings of Biederman et al. (2014), we find that increased understory ET limits the streamflow response to overstory reductions. However, since we assume at least a light understory in forested grid cells, our results attribute this compensatory effect to the understory instead of soil evaporation. In areas where our understory assumption is incorrect, soil evaporation may play a similar role in compensating for overstory ET reductions.

DHSVM results suggest a strong compensation between overstory and understory transpiration in addition to a weaker tradeoff between overstory and understory interception loss (Figure 6). Neglecting increases in understory ET during forest disturbance would lead to about an 86% overestimation of the predicted streamflow response. About 73% of the streamflow response that we do predict is attributable to reductions in canopy interception loss. Understory interception has only a limited capacity for compensation due to lower height and the sheltering effect of remaining trees, both of which contribute to limitations on solar insolation and turbulent vapor transport. Additionally, DHSVM assumes that understory is buried when snow is present in a grid cell, so cold-season precipitation can only be intercepted by the overstory canopy. One limitation of our approach is that the understory maps in DHSVM are updated using a regression model coupled to the LANDIS-II outputs instead of by direct simulation of shrub and herb communities in LANDIS-II. Our results show the importance of improving simulations of multiple vegetation layers and understory regrowth to better constrain compensating ET effects following forest disturbance.

4.4. Uncertainty

A model ensemble derived from multi-objective Bayesian calibration enables the propagation of model parameter uncertainty into our analysis of hydrological responses to forest disturbance. The structure of fully distributed, process-based models like DHSVM is well-suited for extrapolating hydrological interactions to spatially heterogeneous vegetation and climate conditions outside the range of historical observations. However, process-based hydrological models are typically deterministic and challenging to fully constrain with observational data, making uncertainty quantification difficult and threatening the integrity of predictions (e.g., Beven, 1993). By applying a multi-objective Bayesian calibration and selecting an ensemble of Pareto-efficient parameter sets, we are able to estimate model uncertainty and propagate it into our final results (Figures 5 and 7). Despite considerable uncertainty remaining in landscape-scale subsurface parameters (e.g., soil depth and porosity), differences in ensemble model predictions at the sub-watershed scale are roughly an order of magnitude smaller than the size of streamflow generation effects attributable to increased forest disturbance. The grid-scale snowpack response is more uncertain, partially because the configuration of DHSVM used here does not account for sub-grid snow-forest interactions, which can be important in some cases, especially when forest treatments are explicitly targeted toward creating gaps of a certain size (Currier et al., 2022; Sun et al., 2018). Additionally, we do not account for snow transport processes, which leads to discrepancies in the grid-scale spatial pattern of snow accumulation across the landscape (Figures S11 and S12 in Supporting Information S1). Nevertheless, since snow only accounts for 15%–18% of basin-average precipitation in the projected warmer future climate, snowpack uncertainty should only have a limited effect on our water balance findings.

Not all forms of uncertainty can be explicitly represented in our model calibration, and we choose to focus on key processes and parameters identified as sensitive in previous DHSVM studies (e.g., Du et al., 2014). Although our conclusions are robust across two GCMs that are endmembers of fire weather (Maxwell et al., 2022), both GCMs

are downscaled using the same MACA technique (Abatzoglou & Brown, 2012), which may lead to underestimation of future climate uncertainty (Alder & Hostetler, 2018). The MACA downscaling technique, which is based on historical analogs, also may not fully capture the dynamics of future atmospheric river storms (e.g., Gershunov et al., 2019; Huang et al., 2020). There is also the possibility of unforeseen "black swan" events like invasive insects or megafires (Ayars et al., 2023) that could drastically alter the trajectory of forest ecosystems outside the LANDIS-II simulation scope. Despite these modeling limitations, the consistency of our water balance results across multiple calibrated parameter sets and future climate projections should increase confidence in the potential water resource impacts of central Sierra Nevada forest management scenarios.

4.5. Management Implementation

It may be challenging to implement the ongoing landscape-scale disturbance regime contemplated in this study due to high costs. Full restoration of the historic disturbance frequency would require treating ∼6% of the landscape per year for several decades. We emphasize that the scenarios implemented here involve ongoing treatment by thinning and sometimes prescribed fire through the end of the century. Sporadic or temporary treatment campaigns would be unlikely to achieve the level of long-term landscape-scale hydrological response predicted here. Regrowth could compensate for one-time reductions in the overstory, and with limited logistical capacity for simultaneous treatment of different areas, a decadal-scale time horizon is likely required to treat the entire ∼10,000 km^2 landscape even once. Our hydrological results do not show clear separation between treatments using different balances of fire and thinning at a similar overall disturbance frequency (e.g., S3 vs. S4 or S5 vs. S6 in Figure 7). However, distinctions in disturbance type may still be important for snowmelt and ecohydrological processes on sub-annual timescales or smaller spatial scales than considered here. Since we do not adjust model albedo in response to fire, we may underestimate impacts of fire on snowmelt processes (although snow is only 15%–18% of total precipitation).

Moreover, the potential hedge against drought discussed in Section 4.1 is achieved under the fully restored disturbance regime. The partial disturbance scenario (S4) only provides an extra 2%–3% water yield to reservoirs in the 10 driest years, compared to 8%–14% in the full disturbance scenario (S6). This means that full disturbance is about 4–4.7 times more effective at provisioning streamflow, illustrating an economy of scale with respect to the streamflow response to forest disturbance. In other words, more frequent wide-spread disturbance supports a disproportionately larger increase in water provisioning. Compared to the business-as-usual scenario, implementing the full disturbance scenario would represent a considerable increase in the pace and extent of management activities, which would require additional funding. Nevertheless, complementary projects are underway to consider how environmental markets for ecosystem services (including water) and other collaborative initiatives might help enable increases in the pace and scale of forest treatments (Elias et al., 2025; Eriksson et al., 2025; Povak et al., 2024; Quesnel Seipp et al., 2023). Since insect mortality is a large component of tree mortality in all scenarios (see Figure 3 of Maxwell et al. (2022)), unintentional forest reductions from insect mortality and wildfire may still contribute to provisioning increased streamflow in some areas. Additionally, managed wildfire may partially help restore ecosystem diversity and forest structure depending on fire severity and other factors (Boisramé et al., 2017a; Chamberlain et al., 2024; DellaSala et al., 2017). Nevertheless, intentional forest management that achieves a target disturbance return interval can increase the value of ecosystem services that would otherwise be lost (e.g., Chen et al., 2025).

4.6. Transferability

Similar applications of spatially distributed ecohydrological model frameworks can help inform plans for forest and water co-management in other regions. For example, Povak et al. (2022) and Furniss et al. (2023) applied a similar combination of LANDIS-II and DHSVM to simulate the hydrological implications of wildfire and forest treatments in the Cascade Mountains of Washington State, USA, where they similarly found that increased forest disturbance could benefit water-based ecosystem services at least in some areas of the landscape. LANDIS-II is widely applied across diverse global ecosystems to simulate the effects of forest management strategies and climate change (e.g., Cho et al., 2023; Lucash et al., 2023; Mast et al., 2025; Suárez-Muñoz et al., 2023). DHSVM is similarly applied to simulate forest-water interactions across diverse global environments (e.g., Cecílio et al., 2021; Currier et al., 2022; Ridgeway & Surfleet, 2021; Wei et al., 2022), though the hydrologic routing assumptions are best suited for relatively steep topography (i.e., mountain environments). Future studies of forest disturbance may consider using LANDIS-II to create dynamic inputs for DHSVM, as done here, or perhaps

implementing a bidirectional coupling that would enable feedbacks between increased root-zone soil moisture (simulated by DHSVM) and enhanced regrowth (simulated by LANDIS-II). Given the large variability in the streamflow response to forest disturbance (Goeking & Tarboton, 2022), we recommend simulating forest-water interactions in the particular environment where management is planned rather than extrapolating results from other areas.

5. Conclusions

Restoring the pre-colonial landscape-scale forest disturbance frequency shows promise as a hedge against future droughts. In the central Sierra Nevada mountains, distributed hydrological modeling predicts that full restoration of the historic disturbance return interval could produce 8%–14% more inflow into major reservoirs during dry years. Increased streamflow can benefit aquatic and riparian ecosystems, hydropower operations, and municipal or agricultural water customers. In the context of recent Sierra Nevada multi-year droughts (e.g., 2013–2015 and 2020–2022), these benefits may help incentivize investment in central Sierra Nevada forest management. Despite considerable climate-driven uncertainty in the total future water supply (46%–55% difference between GCM projections), the effect of forest disturbance on water yield is relatively well-constrained. In the relatively energy-limited central Sierra Nevada hydroclimate, streamflow gains from increased forest disturbance are partially decoupled from yearly precipitation. Combined with the higher value of water in dry years, this reduced climate sensitivity enhances the value of increased forest disturbance as a potential drought hedge. In a thinner forest, reduced canopy interception and increased snowpack outflow during major storms can increase peak flows in headwaters catchments, but this risk is effectively limited to the scale of smaller road culverts rather than reservoirs. Densely forested sub-watersheds immediately upstream of reservoirs appear most favorable for targeted thinning and fire due to the tradeoff between increased water yield and higher peak flows.

Our study demonstrates the value of linking process-based ecosystem and hydrological models to predict the water resource impacts of landscape-scale forest disturbance frequency. However, extrapolating our results across the western U.S., or even across the Sierra Nevada mountains, is challenging due to the mediating role of aridity, forest type, land cover history, and other factors. Applying similar methods across a wider range of regional climates and forest conditions may help constrain the sensitivity of our results and help prioritize forest management priorities.

Data Availability Statement

Model code and scripts used for running and post-processing results from DHSVM and LANDIS-II are archived at Boardman (2025). The model inputs, outputs, processed results, and other data needed to recreate the results and figures in this study are archived at Boardman (2024).

Acknowledgments
This work was supported by funding from the USDA Forest Service Pacific Southwest Research Station. A. A. Harpold and E. N. Boardman were partially supported by NSF EAR 2012310 and EAR 1723990. E. N. Boardman was additionally supported by the NSF Graduate Research Fellowship Program under Grant 1937966. The authors acknowledge the support of Research & Innovation and the Cyberinfrastructure Team in the Office of Information Technology, especially John Anderson, at the University of Nevada, Reno for facilitation and access to the Pronghorn High-Performance Computing Cluster.

References

Abatzoglou, J. T. (2013). Development of gridded surface meteorological data for ecological applications and modelling. *International Journal of Climatology*, *33*(1), 121–131. https://doi.org/10.1002/joc.3413

Abatzoglou, J. T., & Brown, T. J. (2012). A comparison of statistical downscaling methods suited for wildfire applications. *International Journal of Climatology*, *32*(5), 772–780. https://doi.org/10.1002/joc.2312

Adams, H. D., Luce, C. H., Breshears, D. D., Allen, C. D., Weiler, M., Hale, V. C., et al. (2012). Ecohydrological consequences of drought- and infestation- triggered tree die-off: Insights and hypotheses. *Ecohydrology*, *5*(2), 145–159. https://doi.org/10.1002/eco.233

Alder, J. R., & Hostetler, S. W. (2018). The dependence of hydroclimate projections in snow-dominated regions of the western United States on the choice of statistically downscaled climate data. *Water Resources Research*, *55*(3), 2279–2300. https://doi.org/10.1029/2018WR023458

Andréassian, V. (2004). Waters and forests: From historical controversy to scientific debate. *Journal of Hydrology*, *291*(1), 1–27. https://doi.org/10.1016/j.jhydrol.2003.12.015

Ayars, J., Kramer, H. A., & Jones, G. M. (2023). The 2020 to 2021 California megafires and their impacts on wildlife habitat. *Proceedings of the National Academy of Sciences*, *120*(48), e2312909120. https://doi.org/10.1073/pnas.2312909120

Bales, R. C., Goulden, M. L., Hunsaker, C. T., Conklin, M. H., Hartsough, P. C., O'Geen, A. T., et al. (2018). Mechanisms controlling the impact of multi-year drought on mountain hydrology. *Scientific Reports*, *8*(1), 690. https://doi.org/10.1038/s41598-017-19007-0

Bales, R. C., Molotch, N. P., Painter, T. H., Dettinger, M. D., Rice, R., & Dozier, J. (2006). Mountain hydrology of the western United States. *Water Resources Research*, *42*(8). https://doi.org/10.1029/2005WR004387

Beckers, J., Smerdon, B., & Wilson, M. (2009). Review of hydrologic models for forest management and climate change applications in British Columbia and Alberta. *FORREX Forum for Research and Extension in Natural Resources, Series*, *25*.

Bennett, A., Hamman, J., & Nijssen, B. (2020). MetSim: A Python package for estimation and disaggregation of meteorological data. *Journal of Open Source Software*, *5*(47), 2042. https://doi.org/10.21105/joss.02042

Beven, K. (1993). Prophecy, reality and uncertainty in distributed hydrological modelling. *Advances in Water Resources*, *16*(1), 41–51. https://doi.org/10.1016/0309-1708(93)90028-E

Biederman, J. A., Harpold, A. A., Gochis, D. J., Ewers, B. E., Reed, D. E., Papuga, S. A., & Brooks, P. D. (2014). Increased evaporation following widespread tree mortality limits streamflow response. *Water Resources Research*, *50*(7), 5395–5409. https://doi.org/10.1002/2013WR014994

Biederman, J. A., Somor, A. J., Harpold, A. A., Gutmann, E. D., Breshears, D. D., Troch, P. A., et al. (2015). Recent tree die-off has little effect on streamflow in contrast to expected increases from historical studies. *Water Resources Research*, *51*(12), 9775–9789. https://doi.org/10.1002/2015WR017401

Binois, M., & Picheny, V. (2019). GPareto: An R package for Gaussian-process-based multi-objective optimization and analysis. *Journal of Statistical Software*, *89*(8). https://doi.org/10.18637/jss.v089.i08

Blöschl, G., Bierkens, M. F. P., Chambel, A., Cudennec, C., Destouni, G., Fiori, A., et al. (2019). Twenty-three unsolved problems in hydrology (UPH) – A community perspective. *Hydrological Sciences Journal*, *64*(10), 1141–1158. https://doi.org/10.1080/02626667.2019.1620507

Boardman, E. (2024). Dataset for water resource/forest restoration modeling in Tahoe-central Sierra region [Dataset]. *Zenodo*. https://doi.org/10.5281/zenodo.13984265

Boardman, E. (2025). Code for water resource/forest restoration modeling in Tahoe-central Sierra region [Software]. *Zenodo*. https://doi.org/10.5281/zenodo.14968303

Boisramé, G., Thompson, S., Collins, B., & Stephens, S. (2017). Managed wildfire effects on forest resilience and water in the Sierra Nevada. *Ecosystems*, *20*(4), 717–732. https://doi.org/10.1007/s10021-016-0048-1

Boisramé, G., Thompson, S., & Stephens, S. (2018). Hydrologic responses to restored wildfire regimes revealed by soil moisture-vegetation relationships. *Advances in Water Resources*, *112*, 124–146. https://doi.org/10.1016/j.advwatres.2017.12.009

Boisramé, G. F. S., Thompson, S. E., Kelly, M., Cavalli, J., Wilkin, K. M., & Stephens, S. L. (2017). Vegetation change during 40 years of repeated managed wildfires in the Sierra Nevada, California. *Forest Ecology and Management*, *402*, 241–252. https://doi.org/10.1016/j.foreco.2017.07.034

Boisramé, G. F. S., Thompson, S. E., Tague, C., & Stephens, S. L. (2019). Restoring a natural fire regime alters the water balance of a Sierra Nevada catchment. *Water Resources Research*, *55*(7), 5751–5769. https://doi.org/10.1029/2018WR024098

Boon, S. (2012). Snow accumulation following forest disturbance. *Ecohydrology*, *5*(3), 279–285. https://doi.org/10.1002/eco.212

Bosch, J. M., & Hewlett, J. D. (1982). A review of catchment experiments to determine the effect of vegetation changes on water yield and evapotranspiration. *Journal of Hydrology*, *55*(1), 3–23. https://doi.org/10.1016/0022-1694(82)90117-2

Bowling, L. C., & Lettenmaier, D. P. (2002). *Evaluation of the effects of forest roads on streamflow in hard and ware Creeks, Washington (Technical Report No. 155; water resources series)*. University of Washington.

Burril, E. A., DiTommaso, A. M., Turner, A. M., Pugh, J. A., Christiansen, S. A., & Conkling, B. L. (2021). The forest inventory and analysis database: Database description and user guide [Dataset]. *U.S. Department of Agriculture, Forest Service*. https://research.fs.usda.gov/understory/forest-inventory-and-analysis-database-user-guide-nfi

Cabiyo, B., Fried, J. S., Collins, B. M., Stewart, W., Wong, J., & Sanchez, D. L. (2021). Innovative wood use can enable carbon-beneficial forest management in California. *Proceedings of the National Academy of Sciences*, *118*(49), e2019073118. https://doi.org/10.1073/pnas.2019073118

California Department of Water Resources. (2022). Database of full natural flow records for the AMF, NAT, and YRS stations [Dataset]. *California Data Exchange Center*. https://cdec.water.ca.gov/index.html

Cansler, C. A., Hood, S. M., Varner, J. M., Van Mantgem, P. J., Agne, M. C., Andrus, R. A., et al. (2020). The Fire and Tree Mortality Database, for empirical modeling of individual tree mortality after fire. *Scientific Data*, *7*(1), 194. https://doi.org/10.1038/s41597-020-0522-7

Cecílio, R. A., Oliveira-Ravani, L. T., Zanetti, S. S., & Mendes, H. A. (2021). Method for classifying sites to Atlantic Rainforest restoration aiming to increase basin's streamflows. *iForest: Biogeosciences and Forestry*, *14*(1), 86–94. https://doi.org/10.3832/ifor3658-013

Certini, G. (2005). Effects of fire on properties of forest soils: A review. *Oecologia*, *143*(1), 1–10. https://doi.org/10.1007/s00442-004-1788-8

Chamberlain, C. P., Bartl-Geller, B. N., Cansler, C. A., North, M. P., Meyer, M. D., Van Wagtendonk, L., et al. (2024). When do contemporary wildfires restore forest structures in the Sierra Nevada? *Fire Ecology*, *20*(1), 91. https://doi.org/10.1186/s42408-024-00324-5

Chaney, N. W., Minasny, B., Herman, J. D., Nauman, T. W., Brungard, C. W., Morgan, C. L. S., et al. (2019). POLARIS soil properties: 30-m probabilistic maps of soil properties over the contiguous United States. *Water Resources Research*, *55*(4), 2916–2938. https://doi.org/10.1029/2018WR022797

Chen, H., Sloggy, M. R., Flake, S. W., Evans, S., & Maxwell, C. J. (2025). Impacts of climate-driven insect population change on sawtimber provisioning, carbon sequestration, and water retention: A case study of bark beetle outbreaks in the USA. *Frontiers in Forests and Global Change*, *7*. https://doi.org/10.3389/ffgc.2024.1513721

Cho, W., Lim, W., Choi, W. I., Yang, H. M., & Ko, D. W. (2023). Modeling the effects of forest management scenarios on aboveground biomass and wood production: A study in Mt. Gariwang, South Korea. *Journal of Korean Society of Forest Science*, *112*(2), 173–187. https://doi.org/10.14578/jkfs.2023.112.2.173

Chung, M. G., Guo, H., Nyelele, C., Egoh, B. N., Goulden, M. L., Keske, C. M., & Bales, R. C. (2024). Valuation of forest-management and wildfire disturbance on water and carbon fluxes in mountain headwaters. *Ecohydrology*, *17*(3), e2642. https://doi.org/10.1002/eco.2642

Collins, B. M., Everett, R. G., & Stephens, S. L. (2011). Impacts of fire exclusion and recent managed fire on forest structure in old growth Sierra Nevada mixed-conifer forests. *Ecosphere*, *2*(4), art51. https://doi.org/10.1890/ES11-00026.1

Cuo, L., Lettenmaier, D. P., Mattheussen, B. V., Storck, P., & Wiley, M. (2008). Hydrologic prediction for urban watersheds with the distributed hydrology-soil-vegetation model. *Hydrological Processes*, *22*(21), 4205–4213. https://doi.org/10.1002/hyp.7023

Currier, W. R., Sun, N., Wigmosta, M., Cristea, N., & Lundquist, J. D. (2022). The impact of forest-controlled snow variability on late-season streamflow varies by climatic region and forest structure. *Hydrological Processes*, *36*(6), e14614. https://doi.org/10.1002/hyp.14614

Curtis, J. A., Flint, L. E., Alpers, C. N., & Yarnell, S. M. (2005). Conceptual model of sediment processes in the upper Yuba River watershed, Sierra Nevada, CA. *Geomorphology*, *68*(3), 149–166. https://doi.org/10.1016/j.geomorph.2004.11.019

DellaSala, D. A., Hutto, R. L., Hanson, C. T., Bond, M. L., Ingalsbee, T., Odion, D., & Baker, W. L. (2017). Accommodating mixed-severity fire to restore and maintain ecosystem integrity with a focus on the Sierra Nevada of California, USA. *Fire Ecology*, *13*(2), 148–171. https://doi.org/10.4996/fireecology.130248173

Dewitz, J., & Geological Survey, U. S. (2019). National land cover database (NLCD) 2019 products [Dataset]. *U.S. Geological Survey*. https://doi.org/10.5066/P9JZ7AO3

Dolanc, C. R., Safford, H. D., Thorne, J. H., & Dobrowski, S. Z. (2014). Changing forest structure across the landscape of the Sierra Nevada, CA, USA, since the 1930s. *Ecosphere*, *5*(8), art101-26. https://doi.org/10.1890/ES14-00103.1

Du, E., Link, T. E., Gravelle, J. A., & Hubbart, J. A. (2014). Validation and sensitivity test of the distributed hydrology soil-vegetation model (DHSVM) in a forested mountain watershed. *Hydrological Processes*, *28*(26), 6196–6210. https://doi.org/10.1002/hyp.10110

Dupuy, D., Helbert, C., & Franco, J. (2015). DiceDesign and DiceEval: Two R packages for design and analysis of computer experiments. *Journal of Statistical Software*, *65*(11), 1–38. https://doi.org/10.18637/jss.v065.i11

Eidenshink, J., Schwind, B., Brewer, K., Zhu, Z.-L., Quayle, B., & Howard, S. (2007). A project for monitoring trends in Burn severity. *Fire Ecology*, *3*(1), 3–21. https://doi.org/10.4996/fireecology.0301003

Elias, M., Dees, J., Cabiyo, B., Saksa, P., & Sanchez, D. L. (2023). Financial analysis of innovative wood products and carbon finance to support forest restoration in California. *Forest Products Journal*, *73*(1), 31–42. https://doi.org/10.13073/FPJ-D-22-00049

Elias, M., Yackulic, E., Duffy, K., Saksa, P., Sanchez, D. L., Pevzner, N., et al. (2025). Carbon finance for forest resilience in California. *Frontiers in Forests and Global Change*, *7*. https://doi.org/10.3389/ffgc.2024.1507554

Ellis, C. R., Pomeroy, J. W., Essery, R. L. H., & Link, T. E. (2011). Effects of needleleaf forest cover on radiation and snowmelt dynamics in the Canadian Rocky Mountains. *Canadian Journal of Forest Research*, *41*(3), 608–620. https://doi.org/10.1139/X10-227

Emmerich, M. T. M., Deutz, A. H., & Klinkenberg, J. W. (2011). Hypervolume-based expected improvement: Monotonicity properties and exact computation. In *2011 IEEE congress of evolutionary computation (CEC)* (pp. 2147–2154). https://doi.org/10.1109/CEC.2011.5949880

Eriksson, M., Safeeq, M., Egoh, B., Pathak, T., Lugg, J., O'Geen, A., et al. (2025). The potential of collaborative solutions to improve management of California (United States) wildlands. *Restoration Ecology*, *33*(1), e14330. https://doi.org/10.1111/rec.14330

Farr, T. G., Rosen, P. A., Caro, E., Crippen, R., Duren, R., Hensley, S., et al. (2007). The Shuttle radar topography mission. *Reviews of Geophysics*, *45*(2). https://doi.org/10.1029/2005RG000183

Furniss, T. J., Povak, N. A., Hessburg, P. F., Salter, R. B., Duan, Z., & Wigmosta, M. (2023). Informing climate adaptation strategies using ecological simulation models and spatial decision support tools. *Frontiers in Forests and Global Change*, *6*. https://doi.org/10.3389/ffgc.2023.1269081

Gershunov, A., Shulgina, T., Clemesha, R. E. S., Guirguis, K., Pierce, D. W., Dettinger, M. D., et al. (2019). Precipitation regime change in western North America: The role of atmospheric rivers. *Scientific Reports*, *9*(1), 9944. https://doi.org/10.1038/s41598-019-46169-w

Gilbert, G. K. (1917). *Hydraulic-mining Débris in the Sierra Nevada*. Government Printing Office, Department of the Interior and United States Geological Survey. Professional Paper 105.

Gleason, K. E., McConnell, J. R., Arienzo, M. M., Chellman, N., & Calvin, W. M. (2019). Four-fold increase in solar forcing on snow in western U.S. burned forests since 1999. *Nature Communications*, *10*(1), 2026. https://doi.org/10.1038/s41467-019-09935-y

Gleason, K. E., Nolin, A. W., & Roth, T. R. (2013). Charred forests increase snowmelt: Effects of burned woody debris and incoming solar radiation on snow ablation. *Geophysical Research Letters*, *40*(17), 4654–4661. https://doi.org/10.1002/grl.50896

Goeking, S. A., & Tarboton, D. G. (2020). Forests and water yield: A synthesis of disturbance effects on streamflow and snowpack in western coniferous forests. *Journal of Forestry*, *118*(2), 172–192. https://doi.org/10.1093/jofore/fvz069

Goeking, S. A., & Tarboton, D. G. (2022). Variable streamflow response to forest disturbance in the western US: A large-sample hydrology approach. *Water Resources Research*, *58*(6), e2021WR031575. https://doi.org/10.1029/2021WR031575

Goss, M., Swain, D. L., Abatzoglou, J. T., Sarhadi, A., Kolden, C. A., Williams, A. P., & Diffenbaugh, N. S. (2020). Climate change is increasing the likelihood of extreme autumn wildfire conditions across California. *Environmental Research Letters*, *15*(9), 094016. https://doi.org/10.1088/1748-9326/ab83a7

Guo, H., Goulden, M., Chung, M. G., Nyelele, C., Egoh, B., Keske, C., et al. (2023). Valuing the benefits of forest restoration on enhancing hydropower and water supply in California's Sierra Nevada. *Science of the Total Environment*, *876*, 162836. https://doi.org/10.1016/j.scitotenv.2023.162836

Halofsky, J. E., Peterson, D. L., Buluç, L. Y., & Ko, J. M. (2021). *Climate change vulnerability and adaptation for infrastructure and recreation in the Sierra Nevada (PSW-GTR-272; p. PSW-GTR-272)*. U.S. Department of Agriculture, Forest Service, Pacific Southwest Research Station. https://doi.org/10.2737/PSW-GTR-272

Harpold, A. A., Biederman, J. A., Condon, K., Merino, M., Korgaonkar, Y., Nan, T., et al. (2014). Changes in snow accumulation and ablation following the Las Conchas forest fire, New Mexico, USA. *Ecohydrology*, *7*(2), 440–452. https://doi.org/10.1002/eco.1363

Harpold, A. A., & Kohler, M. (2017). Potential for changing extreme snowmelt and rainfall events in the mountains of the western United States. *Journal of Geophysical Research: Atmospheres*, *122*(24), 13219–13228. https://doi.org/10.1002/2017JD027704

Harpold, A. A., Krogh, S. A., Kohler, M., Eckberg, D., Greenberg, J., Sterle, G., & Broxton, P. D. (2020). Increasing the efficacy of forest thinning for snow using high-resolution modeling: A proof of concept in the lake Tahoe basin, California, USA. *Ecohydrology*, *13*(4), e2203. https://doi.org/10.1002/eco.2203

He, L., Ivanov, V. Y., Bohrer, G., Thomsen, J. E., Vogel, C. S., & Moghaddam, M. (2013). Temporal dynamics of soil moisture in a northern temperate mixed successional forest after a prescribed intermediate disturbance. *Agricultural and Forest Meteorology*, *180*, 22–33. https://doi.org/10.1016/j.agrformet.2013.04.014

Hessburg, P. F., Miller, C. L., Parks, S. A., Povak, N. A., Taylor, A. H., Higuera, P. E., et al. (2019). Climate, environment, and disturbance history govern resilience of western North American forests. *Frontiers in Ecology and Evolution*, *7*. https://doi.org/10.3389/fevo.2019.00239

Hibbert, A. (1967). Forest treatment effects on water yield. In W. A. L. H. Sopper (Ed.), *International symposium on forest hydrology* (pp. 527–543). Pergamon.

Hou, Z., Ren, H., Sun, N., Wigmosta, M. S., Liu, Y., Leung, L. R., et al. (2019). Incorporating climate nonstationarity and snowmelt processes in intensity–duration–frequency analyses with case studies in mountainous areas. *Journal of Hydrometeorology*, *20*(12), 2331–2346. https://doi.org/10.1175/JHM-D-19-0055.1

Huang, X., & Swain, D. L. (2022). Climate change is increasing the risk of a California megaflood. *Science Advances*, *8*(32), eabq0995. https://doi.org/10.1126/sciadv.abq0995

Huang, X., Swain, D. L., & Hall, A. D. (2020). Future precipitation increase from very high resolution ensemble downscaling of extreme atmospheric river storms in California. *Science Advances*, *6*(29), eaba1323. https://doi.org/10.1126/sciadv.aba1323

Hughes, T. F., Latt, C. R., Tappeiner, J. C., II., & Newton, M. (1987). Biomass and Leaf-Area Estimates for Varnishleaf Ceanothus, Deerbrush, and Whiteleaf Manzanita. *Western Journal of Applied Forestry*, *2*(4), 124–128. https://doi.org/10.1093/wjaf/2.4.124

Hungerford, R. D., Nemani, R. R., Running, S. W., & Coughlan, J. C. (1989). MTCLIM: A mountain microclimate simulation model (INT-RP-414; p. INT-RP-414). U.S. Department of Agriculture, Forest Service, Intermountain Forest and Range Experiment Station, Research Paper INT-414. https://doi.org/10.2737/INT-RP-414

Huning, L. S., & Margulis, S. A. (2017). Climatology of seasonal snowfall accumulation across the Sierra Nevada (USA): Accumulation rates, distributions, and variability. *Water Resources Research*, *53*(7), 6033–6049. https://doi.org/10.1002/2017WR020915

Jackson, R. B., Canadell, J., Ehleringer, J. R., Mooney, H. A., Sala, O. E., & Schulze, E. D. (1996). A global analysis of root distributions for terrestrial biomes. *Oecologia*, *108*(3), 389–411. https://doi.org/10.1007/BF00333714

Jones, D. R., Schonlau, M., & Welch, W. J. (1998). Efficient global optimization of expensive black-box functions. *Journal of Global Optimization*, *13*(4), 455–492. https://doi.org/10.1023/A:1008306431147

Jones, J. A., & Grant, G. E. (1996). Peak flow responses to clear-cutting and roads in small and large basins, western cascades, Oregon. *Water Resources Research*, *32*(4), 959–974. https://doi.org/10.1029/95WR03493

Kalies, E. L., & Yocom Kent, L. L. (2016). Tamm review: Are fuel treatments effective at achieving ecological and social objectives? A systematic review. *Forest Ecology and Management*, *375*, 84–95. https://doi.org/10.1016/j.foreco.2016.05.021

Kattelmann, R. C., Berg, N. H., & Rector, J. (1983). The potential for increasing streamflow from Sierra Nevada watersheds. *JAWRA Journal of the American Water Resources Association*, *19*(3), 395–402. https://doi.org/10.1111/j.1752-1688.1983.tb04596.x

Kennedy, J., & Eberhart, R. (1995). Particle swarm optimization. *Proceedings of ICNN '95 - International Conference on Neural Networks*, *4*, 1942–1948. https://doi.org/10.1109/ICNN.1995.488968

King, J. G., & Tennyson, L. C. (1984). Alteration of streamflow characteristics following road construction in North central Idaho. *Water Resources Research*, *20*(8), 1159–1163. https://doi.org/10.1029/WR020i008p01159

Knapp, E. E., Bernal, A. A., Kane, J. M., Fettig, C. J., & North, M. P. (2021). Variable thinning and prescribed fire influence tree mortality and growth during and after a severe drought. *Forest Ecology and Management*, *479*, 118595. https://doi.org/10.1016/j.foreco.2020.118595

Koltunov, A., Ramirez, C. M., Ustin, S. L., Slaton, M., & Haunreiter, E. (2020). eDaRT: The Ecosystem Disturbance and Recovery Tracker system for monitoring landscape disturbances and their cumulative effects. *Remote Sensing of Environment*, *238*, 111482. https://doi.org/10.1016/j.rse.2019.111482

Lewis, G., Harpold, A., Krogh, S. A., Broxton, P., & Manley, P. N. (2023). The prediction of uneven snowpack response to forest thinning informs forest restoration in the central Sierra Nevada. *Ecohydrology*, *16*(7), e2580. https://doi.org/10.1002/eco.2580

Lewis, J., Mori, S. R., Keppeler, E. T., & Ziemer, R. R. (2001). Impacts of logging on storm peak flows, flow volumes and suspended sediment loads in Caspar Creek, California. In M. S. Wigmosta & S. J. Burges (Eds.), *Land use and watersheds: Human influence on hydrology and geomorphology in urban and forest areas. Water science and application* (Vol. 2, pp. 85–125). American Geophysical Union. https://doi.org/10.1029/ws002p0085

Liang, S., Hurteau, M. D., & Westerling, A. L. (2018). Large-scale restoration increases carbon stability under projected climate and wildfire regimes. *Frontiers in Ecology and the Environment*, *16*(4), 207–212. https://doi.org/10.1002/fee.1791

Link, T. E., Unsworth, M., & Marks, D. (2004). The dynamics of rainfall interception by a seasonal temperate rainforest. *Agricultural and Forest Meteorology*, *124*(3), 171–191. https://doi.org/10.1016/j.agrformet.2004.01.010

Loudermilk, E. L., Scheller, R. M., Weisberg, P. J., & Kretchun, A. (2016). Bending the carbon curve: Fire management for carbon resilience under climate change. *Landscape Ecology*, *32*(7), 1461–1472. https://doi.org/10.1007/s10980-016-0447-x

Lucash, M. S., Williams, N. G., Srikrishnan, V., Keller, K., Scheller, R. M., Hegelson, C., et al. (2023). Balancing multiple forest management objectives under climate change in central Wisconsin, U.S.A. *Trees, Forests and People*, *14*, 100460. https://doi.org/10.1016/j.tfp.2023.100460

Ma, S., Concilio, A., Oakley, B., North, M., & Chen, J. (2010). Spatial variability in microclimate in a mixed-conifer forest before and after thinning and burning treatments. *Forest Ecology and Management*, *259*(5), 904–915. https://doi.org/10.1016/j.foreco.2009.11.030

Manley, P. N., Povak, N. A., Wilson, K. N., Fairweather, M. L., Griffey, V., & Long, L. L. (2023). *Blueprint for resilience: The Tahoe-central Sierra initiative (PSW-GTR-277; p. PSW-GTR-277)*. U.S. Department of Agriculture, Forest Service, Pacific Southwest Research Station. https://doi.org/10.2737/PSW-GTR-277

Margulis, S. A., Cortés, G., Girotto, M., & Durand, M. (2016). A Landsat-Era Sierra Nevada Snow Reanalysis (1985–2015). *Journal of Hydrometeorology*, *17*(4), 1203–1221. https://doi.org/10.1175/JHM-D-15-0177.1

Marlon, J. R., Bartlein, P. J., Gavin, D. G., Long, C. J., Anderson, R. S., Briles, C. E., et al. (2012). Long-term perspective on wildfires in the western USA. *Proceedings of the National Academy of Sciences*, *109*(9), E535–E543. https://doi.org/10.1073/pnas.1112839109

Martin, K. A., Van Stan II, J. T., Dickerson-Lange, S. E., Lutz, J. A., Berman, J. W., Gersonde, R., & Lundquist, J. D. (2013). Development and testing of a snow interceptometer to quantify canopy water storage and interception processes in the rain/snow transition zone of the North Cascades, Washington, USA. *Water Resources Research*, *49*(6), 3243–3256. https://doi.org/10.1002/wrcr.20271

Mast, C. N., Williams, N. G., Betts, M. G., & Lucash, M. S. (2025). Land sharing, land sparing, and Triad forestry: Modeling forest composition, diversity, and carbon storage under climate change and natural disturbances. *Landscape Ecology*, *40*(2), 35. https://doi.org/10.1007/s10980-024-02041-5

Maxwell, C. J., Scheller, R. M., Wilson, K. N., & Manley, P. N. (2022). Assessing the effectiveness of landscape-scale forest adaptation actions to improve resilience under projected climate change. *Frontiers in Forests and Global Change*, *5*. https://doi.org/10.3389/ffgc.2022.740869

McMichael, C. E., Hope, A. S., Roberts, D. A., & Anaya, M. R. (2004). Post-fire recovery of leaf area index in California chaparral: A remote sensing-chronosequence approach. *International Journal of Remote Sensing*, *25*(21), 4743–4760. https://doi.org/10.1080/01431160410001726067

Meili, N., Beringer, J., Zhao, J., & Fatichi, S. (2024). Aerodynamic effects cause higher forest evapotranspiration and water yield reductions after wildfires in tall forests. *Global Change Biology*, *30*(1), e16995. https://doi.org/10.1111/gcb.16995

Mijic, A., Liu, L., O'Keeffe, J., Dobson, B., & Chun, K. P. (2024). A meta-model of socio-hydrological phenomena for sustainable water management. *Nature Sustainability*, *7*(1), 7–14. https://doi.org/10.1038/s41893-023-01240-3

Moore, G. W., & Heilman, J. L. (2011). Proposed principles governing how vegetation changes affect transpiration. *Ecohydrology*, *4*(3), 351–358. https://doi.org/10.1002/eco.232

Moore, R., & Wondzell, S. M. (2005). Physical Hydrology and the effects of forest harvesting in the Pacific Northwest: A review. *JAWRA Journal of the American Water Resources Association*, *41*(4), 763–784. https://doi.org/10.1111/j.1752-1688.2005.tb04463.x

Morecroft, M. D., Taylor, M. E., & Oliver, H. R. (1998). Air and soil microclimates of deciduous woodland compared to an open site. *Agricultural and Forest Meteorology*, *90*(1), 141–156. https://doi.org/10.1016/S0168-1923(97)00070-1

Morris, M. D., & Mitchell, T. J. (1995). Exploratory designs for computational experiments. *Journal of Statistical Planning and Inference*, *43*(3), 381–402. https://doi.org/10.1016/0378-3758(94)00035-T

National Interagency Fire Center. (2019). Historic Fire Perimeters [Dataset]. https://data-nifc.opendata.arcgis.com/search?tags=fire_progression_opendata%2CCategory

North, M., Innes, J., & Zald, H. (2007). Comparison of thinning and prescribed fire restoration treatments to Sierran mixed-conifer historic conditions. *Canadian Journal of Forest Research*, *37*(2), 331–342. https://doi.org/10.1139/X06-236

Patton, N. R., Lohse, K. A., Godsey, S. E., Crosby, B. T., & Seyfried, M. S. (2018). Predicting soil thickness on soil mantled hillslopes. *Nature Communications*, *9*(1), 3329. Article 1. https://doi.org/10.1038/s41467-018-05743-y

Perry, T. D., & Jones, J. A. (2016). Summer streamflow deficits from regenerating Douglas-fir forest in the Pacific Northwest, USA. *Ecohydrology*, *10*(2), e1790. https://doi.org/10.1002/eco.1790

Piske, C. R., Carroll, R., Boisrame, G., Krogh, S. A., Manning, A. L., Underwood, K. L., et al. (2024). Lidar-Derived Forest Metrics Predict Snow Accumulation and Ablation in the Central Sierra Nevada, USA. *Authorea*. [Preprint]. https://doi.org/10.22541/au.171799893.36954583/v1

Pomeroy, J., Fang, X., & Ellis, C. (2012). Sensitivity of snowmelt hydrology in Marmot Creek, Alberta, to forest cover disturbance. *Hydrological Processes*, *26*(12), 1891–1904. https://doi.org/10.1002/hyp.9248

Povak, N. A., Furniss, T. J., Hessburg, P. F., Salter, R. B., Wigmosta, M., Duan, Z., & LeFevre, M. (2022). Evaluating Basin-Scale Forest Adaptation Scenarios: Wildfire, Streamflow, Biomass, and Economic Recovery Synergies and Trade-Offs. *Frontiers in Forests and Global Change*, *5*. https://doi.org/10.3389/ffgc.2022.805179

Povak, N. A., Manley, P. N., & Wilson, K. N. (2024). Quantitative methods for integrating climate adaptation strategies into spatial decision support models. *Frontiers in Forests and Global Change*, *7*. https://doi.org/10.3389/ffgc.2024.1286937

PRISM Climate Group. (2022). PRISM Gridded Climate Data, 800 m Normals [Dataset]. *Oregon State University*. https://prism.oregonstate.edu

Quesnel Seipp, K., Maurer, T., Elias, M., Saksa, P., Keske, C., Oleson, K., et al. (2023). A multi-benefit framework for funding forest management in fire-driven ecosystems across the Western U.S. *Journal of Environmental Management*, *344*, 118270. https://doi.org/10.1016/j.jenvman.2023.118270

Rambo, T. R., & North, M. P. (2009). Canopy microclimate response to pattern and density of thinning in a Sierra Nevada forest. *Forest Ecology and Management*, *257*(2), 435–442. https://doi.org/10.1016/j.foreco.2008.09.029

Rasmussen, C. E., & Williams, C. K. I. (2008). *Gaussian processes for machine learning*. MIT Press.

Ridgeway, J. B., & Surfleet, C. G. (2021). Effects of Streamside Buffers on Stream Temperatures Associated With Forest Management and Harvesting Using DHSVM-RBM; South Fork Caspar Creek, California. *Frontiers in Forests and Global Change*, *4*. https://doi.org/10.3389/ffgc.2021.611380

Roche, J. W., Goulden, M. L., & Bales, R. C. (2018). Estimating evapotranspiration change due to forest treatment and fire at the basin scale in the Sierra Nevada, California. *Ecohydrology*, *11*(7), e1978. https://doi.org/10.1002/eco.1978

Roche, J. W., Ma, Q., Rungee, J., & Bales, R. C. (2020). Evapotranspiration Mapping for Forest Management in California's Sierra Nevada. *Frontiers in Forests and Global Change*, *3*. https://doi.org/10.3389/ffgc.2020.00069

Roustant, O., Ginsbourger, D., & Deville, Y. (2012). DiceKriging, DiceOptim: Two R Packages for the Analysis of Computer Experiments by Kriging-Based Metamodeling and Optimization. *Journal of Statistical Software*, *51*, 1–55. https://doi.org/10.18637/jss.v051.i01

Safa, H., Krogh, S. A., Greenberg, J., Kostadinov, T. S., & Harpold, A. A. (2021). Unraveling the Controls on Snow Disappearance in Montane Conifer Forests Using Multi-Site Lidar. *Water Resources Research*, *57*(12), e2020WR027522. https://doi.org/10.1029/2020WR027522

Safford, H. D., Paulson, A. K., Steel, Z. L., Young, D. J. N., & Wayman, R. B. (2022). The 2020 California fire season: A year like no other, a return to the past or a harbinger of the future? *Global Ecology and Biogeography*, *31*(10), 2005–2025. https://doi.org/10.1111/geb.13498

Saksa, P. C., Bales, R. C., Tague, C. L., Battles, J. J., Tobin, B. W., & Conklin, M. h. (2020). Fuels treatment and wildfire effects on runoff from Sierra Nevada mixed-conifer forests. *Ecohydrology*, *13*(3), e2151. https://doi.org/10.1002/eco.2151

Saksa, P. C., Conklin, M. H., Battles, J. J., Tague, C. L., & Bales, R. C. (2017). Forest thinning impacts on the water balance of Sierra Nevada mixed-conifer headwater basins. *Water Resources Research*, *53*(7), 5364–5381. https://doi.org/10.1002/2016WR019240

Scheller, R., Kretchun, A., Hawbaker, T. J., & Henne, P. D. (2019). A landscape model of variable social-ecological fire regimes. *Ecological Modelling*, *401*, 85–93. https://doi.org/10.1016/j.ecolmodel.2019.03.022

Scheller, R. M., Domingo, J. B., Sturtevant, B. R., Williams, J. S., Rudy, A., Gustafson, E. J., & Mladenoff, D. J. (2007). Design, development, and application of LANDIS-II, a spatial landscape simulation model with flexible temporal and spatial resolution. *Ecological Modelling*, *201*(3–4), 409–419. https://doi.org/10.1016/j.ecolmodel.2006.10.009

Scheller, R. M., Hua, D., Bolstad, P. V., Birdsey, R. A., & Mladenoff, D. J. (2011). The effects of forest harvest intensity in combination with wind disturbance on carbon dynamics in Lake States Mesic Forests. *Ecological Modelling*, *222*(1), 144–153. https://doi.org/10.1016/j.ecolmodel.2010.09.009

Scheller, R. M., Kretchun, A. M., Loudermilk, E. L., Hurteau, M. D., Weisberg, P. J., & Skinner, C. (2018). Interactions among fuel management, species composition, bark beetles, and climate change and the potential effects on forests of the Lake Tahoe Basin. *Ecosystems*, *21*(4), 643–656. https://doi.org/10.1007/s10021-017-0175-3

Schoennagel, T., Balch, J. K., Brenkert-Smith, H., Dennison, P. E., Harvey, B. J., Krawchuk, M. A., et al. (2017). Adapt to more wildfire in western North American forests as climate changes. *Proceedings of the National Academy of Sciences*, *114*(18), 4582–4590. https://doi.org/10.1073/pnas.1617464114

Scholl, A. E., & Taylor, A. H. (2010). Fire regimes, forest change, and self-organization in an old-growth mixed-conifer forest, Yosemite National Park, USA. *Ecological Applications*, *20*(2), 362–380. https://doi.org/10.1890/08-2324.1

Schwalm, C. R., Glendon, S., & Duffy, P. B. (2020). RCP8.5 tracks cumulative CO_2 emissions. *Proceedings of the National Academy of Sciences*, *117*(33), 19656–19657. https://doi.org/10.1073/pnas.2007117117

Seidl, R., Thom, D., Kautz, M., Martin-Benito, D., Peltoniemi, M., Vacchiano, G., et al. (2017). Forest disturbances under climate change. *Nature Climate Change*, *7*(6), 395–402. https://doi.org/10.1038/nclimate3303

Sen, P. K. (1968). Estimates of the regression coefficient based on Kendall's Tau. *Journal of the American Statistical Association*, *63*(324), 1379–1389. https://doi.org/10.1080/01621459.1968.10480934

Short, K. C. (2021). Spatial wildfire occurrence data for the United States, 1992-2018 [FPA_FOD_20210617] 5th Edition [Dataset]. https://doi.org/10.2737/RDS-2013-0009.5

Skinner, C. N., & Chang, C. (1996). Fire regimes, past and present. In *Sierra Nevada ecosystem project: Final report to congress. Vol. II. Assessments and scientific basis for management options. Wildland resources center report No. 37. Centers for water and wildland resources* (Vol. 2, pp. 1041–1069). University of California, Davis.

Soil, S. S. (2022). Soil Survey geographic (SSURGO) database [Dataset]. *Natural Resources Conservation Service, United States Department of Agriculture*. https://sdmdataaccess.sc.egov.usda.gov

Startsev, A. D., & McNabb, D. H. (2000). Effects of skidding on forest soil infiltration in west-central Alberta. *Canadian Journal of Soil Science*, *80*(4), 617–624. https://doi.org/10.4141/S99-092

Steel, Z. L., Safford, H. D., & Viers, J. H. (2015). The fire frequency-severity relationship and the legacy of fire suppression in California forests. *Ecosphere*, *6*(1), art8–23. https://doi.org/10.1890/ES14-00224.1

Stephens, S. L., Battaglia, M. A., Churchill, D. J., Collins, B. M., Coppoletta, M., Hoffman, C. M., et al. (2021). Forest restoration and fuels reduction: Convergent or divergent? *BioScience*, *71*(1), 85–101. https://doi.org/10.1093/biosci/biaa134

Stephens, S. L., Collins, B. M., Biber, E., & Fulé, P. Z. (2016). U.S. federal fire and forest policy: Emphasizing resilience in dry forests. *Ecosphere*, *7*(11), e01584. https://doi.org/10.1002/ecs2.1584

Stephens, S. L., Thompson, S., Boisramé, G., Collins, B. M., Ponisio, L. C., Rakhmatulina, E., et al. (2021). Fire, water, and biodiversity in the Sierra Nevada: A possible triple win. *Environmental Research Communications*, *3*(8), 081004. https://doi.org/10.1088/2515-7620/ac17e2

Stevens, J. T. (2017). Scale-dependent effects of post-fire canopy cover on snowpack depth in montane coniferous forests. *Ecological Applications*, *27*(6), 1888–1900. https://doi.org/10.1002/eap.1575

Storck, P., Lettenmaier, D. P., & Bolton, S. M. (2002). Measurement of snow interception and canopy effects on snow accumulation and melt in a mountainous maritime climate, Oregon, United States. *Water Resources Research*, *38*(11). https://doi.org/10.1029/2002WR001281

Sturtevant, B. R., Gustafson, E. J., Li, W., & He, H. S. (2004). Modeling biological disturbances in LANDIS: A module description and demonstration using spruce budworm. *Ecological Modelling*, *180*(1), 153–174. https://doi.org/10.1016/j.ecolmodel.2004.01.021

Suárez-Muñoz, M., Bonet-García, F. J., Navarro-Cerrillo, R., Herrero, J., & Mina, M. (2023). Forest management scenarios drive future dynamics of Mediterranean planted pine forests under climate change. *Landscape Ecology*, *38*(8), 2069–2084. https://doi.org/10.1007/s10980-023-01678-y

Sun, G., Wei, X., Hao, L., Sanchis, M. G., Hou, Y., Yousefpour, R., et al. (2023). Forest hydrology modeling tools for watershed management: A review. *Forest Ecology and Management*, *530*, 120755. https://doi.org/10.1016/j.foreco.2022.120755

Sun, N., Wigmosta, M., Zhou, T., Lundquist, J., Dickerson-Lange, S., & Cristea, N. (2018). Evaluating the functionality and streamflow impacts of explicitly modelling forest–snow interactions and canopy gaps in a distributed hydrologic model. *Hydrological Processes*, *32*(13), 2128–2140. https://doi.org/10.1002/hyp.13150

Sun, N., Yan, H., Wigmosta, M. S., Leung, L. R., Skaggs, R., & Hou, Z. (2019). Regional Snow Parameters Estimation for Large-Domain Hydrological Applications in the Western United States. *Journal of Geophysical Research: Atmospheres*, *124*(10), 5296–5313. https://doi.org/10.1029/2018JD030140

Swezy, C., Bailey, J., & Chung, W. (2021). Linking Federal Forest Restoration with Wood Utilization: Modeling Biomass Prices and Analyzing Forest Restoration Costs in the Northern Sierra Nevada. *Energies*, *14*(9), 2696. Article 9. https://doi.org/10.3390/en14092696

Tague, C., & Dugger, A. L. (2010). Ecohydrology and Climate Change in the Mountains of the Western USA – A Review of Research and Opportunities. *Geography Compass*, *4*(11), 1648–1663. https://doi.org/10.1111/j.1749-8198.2010.00400.x

Taylor, A. H., Vandervlugt, A. M., Maxwell, R. S., Beaty, R. M., Airey, C., & Skinner, C. N. (2014). Changes in forest structure, fuels and potential fire behaviour since 1873 in the Lake Tahoe Basin, USA. *Applied Vegetation Science*, *17*(1), 17–31. https://doi.org/10.1111/avsc.12049

Tennant, C. J., Harpold, A. A., Lohse, K. A., Godsey, S. E., Crosby, B. T., Larsen, L. G., et al. (2017). Regional sensitivities of seasonal snowpack to elevation, aspect, and vegetation cover in western North America. *Water Resources Research*, *53*(8), 6908–6926. https://doi.org/10.1002/2016WR019374

Thomas, R. B., & Megahan, W. F. (1998). Peak flow responses to clear-cutting and roads in small and large basins, Western Cascades, Oregon: A second opinion. *Water Resources Research*, *34*(12), 3393–3403. https://doi.org/10.1029/98WR02500

Troendle, C. A. (1979). Effect of timber harvest on water yield and timing of runoff—Snow region. U.S. Department of Agriculture Forest Service Pacific Northwest Forest and Range Experiment Station. Retrieved from http://archive.org/details/CAT83778580

Troendle, C. A. (1983). The Potential for Water Yield Augmentation from Forest Management in the Rocky Mountain Region. *JAWRA Journal of the American Water Resources Association*, *19*(3), 359–373. https://doi.org/10.1111/j.1752-1688.1983.tb04593.x

Troendle, C. A., & King, R. M. (1985). The Effect of Timber Harvest on the Fool Creek Watershed, 30 Years Later. *Water Resources Research*, *21*(12), 1915–1922. https://doi.org/10.1029/WR021i012p01915

U.S. Department of the Interior, Geological Survey, and U.S. Department of Agriculture. (2016). LANDFIRE dataset [Dataset]. http://www.landfire/viewer

U.S. Geological Survey. (2019). National Hydrography Dataset [Dataset]. https://www.usgs.gov/national-hydrography/access-national-hydrography-products

U.S. Geological Survey. (2022). National Water Information System daily streamflow data for sites 103366092, 10336610, 10336645, 10336660, 10336676, 10336730, 10336780, 10343500, 11413000, 11413300, 11427000, 11427700 [Dataset]. http://waterdata.usgs.gov/nwis/

van Wagtendonk, J. W., Fites-Kaufman, J. A., Safford, H. D., North, M. P., & Collins, B. M. (2018). Sierra Nevada Bioregion. In J. W. van Wagtendonk, N. G. Sugihara, S. L. Stephens, A. E. Thode, K. E. Shaffer, & J. A. Fites-Kaufman (Eds.), *Fire in California's ecosystems* (pp. 249–278). University of California Press. https://doi.org/10.1525/california/9780520246058.003.0012

Varhola, A., Coops, N. C., Weiler, M., & Moore, R. D. (2010). Forest canopy effects on snow accumulation and ablation: An integrative review of empirical results. *Journal of Hydrology*, *392*(3), 219–233. https://doi.org/10.1016/j.jhydrol.2010.08.009

Vogel, R. M., & Fennessey, N. M. (1995). Flow Duration Curves II: A Review of Applications in Water Resources Planning. *JAWRA Journal of the American Water Resources Association*, *31*(6), 1029–1039. https://doi.org/10.1111/j.1752-1688.1995.tb03419.x

Voldoire, A., Sanchez-Gomez, E., Salas y Mélia, D., Decharme, B., Cassou, C., Sénési, S., et al. (2013). The CNRM-CM5.1 global climate model: Description and basic evaluation. *Climate Dynamics*, *40*(9), 2091–2121. https://doi.org/10.1007/s00382-011-1259-y

Watanabe, M., Suzuki, T., O'ishi, R., Komuro, Y., Watanabe, S., Emori, S., et al. (2010). Improved Climate Simulation by MIROC5: Mean States, Variability, and Climate Sensitivity. *Journal of Climate*, *23*(23), 6312–6335. https://doi.org/10.1175/2010JCLI3679.1

Wei, L., Qiu, Z., Zhou, G., Zuecco, G., Liu, Y., & Wen, Y. (2022). Soil water hydraulic redistribution in a subtropical monsoon evergreen forest. *Science of the Total Environment*, *835*, 155437. https://doi.org/10.1016/j.scitotenv.2022.155437

Wigmosta, M. S., Nijssen, B., & Storck, P. (2002). The Distributed Hydrology Soil Vegetation Model. In V. P. Singh & D. K. Frevert (Eds.), *Mathematical models of small watershed hydrology and applications* (pp. 7–42). Water Resources Publications, LLC.

Wigmosta, M. S., Vail, L. W., & Lettenmaier, D. P. (1994). A distributed hydrology-vegetation model for complex terrain. *Water Resources Research*, *30*(6), 1665–1679. https://doi.org/10.1029/94WR00436

Winkler, R., Boon, S., Zimonick, B., & Spittlehouse, D. (2012). Snow accumulation and ablation response to changes in forest structure and snow surface albedo after attack by mountain pine beetle. *Hydrological Processes*, *28*(2), 197–209. https://doi.org/10.1002/hyp.9574

Yuba Water Agency. (2023). Atmospheric River Control Spillway at New Bullards Bar Dam. Retrieved from https://www.yubawater.org/252/ARC-Spillway-at-New-Bullards-Bar-Dam

Zambrano-Bigiarini, M., & Rojas, R. (2013). A model-independent Particle Swarm Optimisation software for model calibration. *Environmental Modelling & Software*, *43*, 5–25. https://doi.org/10.1016/j.envsoft.2013.01.004

Zeller, K. A., Povak, N. A., Manley, P., Flake, S. W., & Hefty, K. L. (2023). Managing for biodiversity: The effects of climate, management and natural disturbance on wildlife species richness. *Diversity and Distributions*, *29*(12), 1623–1638. https://doi.org/10.1111/ddi.13782

References From the Supporting Information

Adler, A. (2015). lamW: Lambert-W Function (Version R package version 2.1.1) [Computer software]. https://doi.org/10.5281/zenodo.5874874

Alberti, M., Weeks, R., & Coe, S. (2004). Urban land-cover change analysis in central puget sound. *Photogrammetric Engineering & Remote Sensing*, *70*(9), 1043–1052. https://doi.org/10.14358/PERS.70.9.1043

Bieger, K., Rathjens, H., Allen, P. M., & Arnold, J. G. (2015). Development and evaluation of bankfull hydraulic geometry relationships for the physiographic regions of the United States. *JAWRA Journal of the American Water Resources Association*, *51*(3), 842–858. https://doi.org/10.1111/jawr.12282

Brooks, R. H., & Corey, A. T. (1964). Hydraulic properties of porous media and their relation to drainage design. *Transactions of the ASAE*, *7*(1), 0026–0028. https://doi.org/10.13031/2013.40684
Carter, G. A., Smith, W. K., & Hadley, J. L. (1988). Stomatal conductance in three conifer species at different elevations during summer in Wyoming. *Canadian Journal of Forest Research*, *18*(2), 242–246. https://doi.org/10.1139/x88-035
Cirelli, D., Equiza, M. A., Lieffers, V. J., & Tyree, M. T. (2015). Populus species from diverse habitats maintain high night-time conductance under drought. *Tree Physiology*, *tpv092*, tpv092. https://doi.org/10.1093/treephys/tpv092
Conard, S. G., Sparks, S. R., & Regelbrugge, J. C. (1997). Comparative plant water relations and soil water depletion patterns of three seral shrub species on forest sites in Southwestern Oregon. *Forest Science*, *43*(3), 336–347. https://doi.org/10.1093/forestscience/43.3.336
Corless, R. M., Gonnet, G. H., Hare, D. E. G., Jeffrey, D. J., & Knuth, D. E. (1996). On the LambertW function. *Advances in Computational Mathematics*, *5*(1), 329–359. https://doi.org/10.1007/BF02124750
DeLucia, E. H., & Schlesinger, W. H. (1991). Resource-use efficiency and drought tolerance in adjacent great basin and Sierran plants. *Ecology*, *72*(1), 51–58. https://doi.org/10.2307/1938901
Denmead, O. T., & Millar, B. D. (1976). Field studies of the conductance of wheat leaves and transpiration. *Agronomy Journal*, *68*(2), 307–311. https://doi.org/10.2134/agronj1976.00021962006800020026x
Dickinson, R., Henderson-Sellers, A., & Kennedy, P. (1993). *Biosphere-atmosphere Transfer Scheme (BATS) Version 1e as Coupled to the NCAR Community Climate Model* (p. 3040). UCAR/NCAR. https://doi.org/10.5065/D67W6959
Farouki, O. T. (1981). The thermal properties of soils in cold regions. *Cold Regions Science and Technology*, *5*(1), 67–75. https://doi.org/10.1016/0165-232X(81)90041-0
Fetcher, N. (1976). Patterns of leaf resistance to lodgepole pine transpiration in wyoming. *Ecology*, *57*(2), 339–345. https://doi.org/10.2307/1934822
Hinckley, T. M., Lassoie, J. P., & Running, S. W. (1978). Temporal and spatial variations in the water status of forest trees. *Forest Science*, *20*.
Kattelmann, R. (1990). Variability of liquid water content in an alpine snowpack. In *International snow science workshop proceedings* (pp. 261–265). Montana State University Library. Retrieved from http://arc.lib.montana.edu/snow-science/item/689
Knapp, A. K., & Smith, W. K. (1987). Stomatal and photosynthetic responses during sun/shade transitions in subalpine plants: Influence on water use efficiency. *Oecologia*, *74*(1), 62–67. https://doi.org/10.1007/BF00377346
Knauer, J., El-Madany, T. S., Zaehle, S., & Migliavacca, M. (2018). Bigleaf—An R package for the calculation of physical and physiological ecosystem properties from eddy covariance data. *PLoS One*, *13*(8), e0201114. https://doi.org/10.1371/journal.pone.0201114
Koç, İ. (2019). *Conifers response to water stress: Physiological responses and effects on nutrient use physiology* (PhD Dissertation). Michigan State University. https://doi.org/10.25335/qx4f-7y36
Kummerow, J., Krause, D., & Jow, W. (1977). Root systems of chaparral shrubs. *Oecologia*, *29*(2), 163–177. https://doi.org/10.1007/BF00345795
Law, B. E. (1995). Estimation of leaf area index and light intercepted by shrubs from digital videography. *Remote Sensing of Environment*, *51*(2), 276–280. https://doi.org/10.1016/0034-4257(94)00054-Q
Link, T. E., & Marks, D. (1999). Point simulation of seasonal snow cover dynamics beneath boreal forest canopies. *Journal of Geophysical Research*, *104*(D22), 27841–27857. https://doi.org/10.1029/1998JD200121
Mahat, V., & Tarboton, D. G. (2012). Canopy radiation transmission for an energy balance snowmelt model: Canopy radiation for snowmelt. *Water Resources Research*, *48*(1). https://doi.org/10.1029/2011WR010438
Marks, D., Kimball, J., Tingey, D., & Link, T. (1998). The sensitivity of snowmelt processes to climate conditions and forest cover during rain-on-snow: A case study of the 1996 Pacific Northwest flood. *Hydrological Processes*, *12*(10–11), 1569–1587. https://doi.org/10.1002/(SICI)1099-1085(199808/09)12:10/11<1569::AID-HYP682>3.0.CO;2-L
Matzner, S. L., Rice, K. J., & Richards, J. H. (2003). Patterns of stomatal conductance among blue oak (Quercus douglasii) size classes and populations: Implications for seedling establishment. *Tree Physiology*, *23*(11), 777–784. https://doi.org/10.1093/treephys/23.11.777
McDowell, N. G., Phillips, N., Lunch, C., Bond, B. J., & Ryan, M. G. (2002). An investigation of hydraulic limitation and compensation in large, old Douglas-fir trees. *Tree Physiology*, *22*(11), 763–774. https://doi.org/10.1093/treephys/22.11.763
Moeys, J. (2018). The soil texture wizard: R functions for plotting, classifying, transforming and exploring soil texture data [Computer Software]. https://cran.r-project.org/web/packages/soiltexture/vignettes/soiltexture_vignette.pdf
Monson, R. K., & Grant, M. C. (1989). Experimental studies of ponderosa pine. III. Differences in photosynthesis, stomatal conductance, and water-use efficiency between two genetic lines. *American Journal of Botany*, *76*(7), 1041–1047. https://doi.org/10.1002/j.1537-2197.1989.tb15085.x
Renninger, H. J., Carlo, N., Clark, K. L., & Schafer, K. V. R. (2014). Physiological strategies of co-occurring oaks in a water- and nutrient-limited ecosystem. *Tree Physiology*, *34*(2), 159–173. https://doi.org/10.1093/treephys/tpt122
Riikonen, J., Kets, K., Darbah, J., Oksanen, E., Sober, A., Vapaavuori, E., et al. (2008). Carbon gain and bud physiology in *Populus tremuloides* and *Betula papyrifera* grown under long-term exposure to elevated concentrations of CO2 and O3. *Tree Physiology*, *28*(2), 243–254. https://doi.org/10.1093/treephys/28.2.243
Rood, S. B., Bigelow, S. G., & Hall, A. A. (2011). Root architecture of riparian trees: River cut-banks provide natural hydraulic excavation, revealing that cottonwoods are facultative phreatophytes. *Trees*, *25*(5), 907–917. https://doi.org/10.1007/s00468-011-0565-7
Ross, K. M., & Loik, M. E. (2021). Photosynthetic sensitivity to historic meteorological variability for conifers in the eastern Sierra Nevada. *International Journal of Biometeorology*, *65*(6), 851–863. https://doi.org/10.1007/s00484-020-02062-0
Running, S. W. (1976). Environmental control of leaf water conductance in conifers. *Canadian Journal of Forest Research*, *6*(1), 104–112. https://doi.org/10.1139/x76-013
Sala, A., Carey, E. V., Keane, R. E., & Callaway, R. M. (2001). Water use by whitebark pine and subalpine fir: Potential consequences of fire exclusion in the northern Rocky Mountains. *Tree Physiology*, *21*(11), 717–725. https://doi.org/10.1093/treephys/21.11.717
Shuttleworth, J. W. (1993). Evaporation. In D. R. Maidment (Ed.), *Handbook of hydrology* (pp. 98–144). McGraw-Hill.
Steele, S. J., Gower, S. T., Vogel, J. G., & Norman, J. M. (1997). Root mass, net primary production and turnover in aspen, jack pine and black spruce forests in Saskatchewan and Manitoba, Canada. *Tree Physiology*, *17*(8–9), 577–587. https://doi.org/10.1093/treephys/17.8-9.577
Svejcar, T., & Riegel, G. M. (1998). Spatial pattern of gas exchange for montane moist meadow species. *Journal of Vegetation Science*, *9*(1), 85–94. https://doi.org/10.2307/3237226
Tan, C.-S. (1977). *A study of stomatal diffusion resistance in a Douglas fir forest* (PhD Dissertation). The University of British Columbia. http://resolve.library.ubc.ca/cgi-bin/catsearch?bid=1565303
Thyer, M., Beckers, J., Spittlehouse, D., Alila, Y., & Winkler, R. (2004). Diagnosing a distributed hydrologic model for two high-elevation forested catchments based on detailed stand- and basin-scale data. *Water Resources Research*, *40*(1). https://doi.org/10.1029/2003WR002414
van Genuchten, M. T. (1980). A Closed-form Equation for Predicting the Hydraulic Conductivity of Unsaturated Soils. *Soil Science Society of America Journal*, *44*(5), 892–898. https://doi.org/10.2136/sssaj1980.03615995004400050002x

van Heeswijk, M., Kimball, J. S., & Marks, D. (1996). Simulation of water available for runoff in clearcut forest openings during rain-on-snow events in the western Cascade Range of Oregon and Washington. U.S. Geological Survey Water-Resources Investigations Report 95-4219. https://doi.org/10.3133/wri954219

Wolfram Research. (1988). Solve, Wolfram Language function (Version Updated 2020). [Computer software]. https://reference.wolfram.com/language/ref/Solve.html

Yoder, B. J. (1983). *Comparative water relations of* Abies grandis, Abies concolor *and their hybrids* (Masters Thesis). Oregon State University. https://ir.library.oregonstate.edu/concern/graduate_thesis_or_dissertations/wh246x36p